AN EXPERIMENTAL INVESTIGATION OF ACOUSTIC CAVITATION AS A FRAGMENTATION MECHANISM OF MOLTEN TIN DROPLETS IN WATER

by

TROND ARNOLD BJORNARD

B.A., Kalamazoo College
(1971)

SUBMITTED IN PARTIAL FULFILLMENT

OF THE REQUIREMENTS FOR THE

DEGREE OF MASTER OF

SCIENCE

at the

MASSACHUSETTS INSTITUTE OF TECHNOLOGY

SEPTEMBER, 1975
(i.e. February 1976)

Signature of Author _____
Department of Nuclear Engineering, September, 1975

Certified by _____
Thesis Supervisor

Accepted by _____
Chairman, Departmental Committee on Graduate Students

Archives

MASS. INST. TECH.
FEB 24 1976
LIBRARIES

AN EXPERIMENTAL INVESTIGATION OF ACOUSTIC CAVITATION AS A FRAGMENTATION MECHANISM OF MOLTEN TIN DROPLETS IN WATER

by

TROND ARNOLD BJORNARD

Submitted to the Department of Nuclear Engineering on September 26, 1975, in partial fulfillment of the requirements for the degree of Master of Science.

ABSTRACT

A series of experiments were performed where single molten tin droplets of known size, shape and temperature were dropped from a low height into a pool of distilled water. The pressure waves emanating from the hot droplets were recorded by a transducer located in the coolant for varying initial droplet and pool temperatures.

The pressure results obtained show well defined patterns of pressure frequency and magnitude behavior. Application of the results to the acoustic cavitation theory of fragmentation shows that the pressure excursions within the molten tin are considerably less severe than was predicted. The likelihood that acoustic cavitation caused the observed fragmentation is therefore considerably diminished.

Further, the results strongly suggest that spontaneous nucleation of the coolant did not cause the observed fragmentation, while it appears that another mechanism linked to the observed dwell time behavior was responsible. Further theoretical and experimental work is required to establish the nature of this mechanism.

Thesis Supervisor: Neil E. Todreas
Title: Professor of Nuclear Engineering

ACKNOWLEDGEMENTS

This work was sponsored by Argonne National Laboratory and the U.S. Atomic Energy Commission.

Assistance provided through discussions with the following people was most helpful - Glenn Bjorkquist, Dave Gwinn, Dr. Mujid Kazimi, Roland Knapp, Professor David Lanning, Professor Warren Rohsenow, and Dr. Charles Watson.

Special appreciation is extended to Professor Neil E. Todreas for his able and invaluable guidance and direction.

TABLE OF CONTENTS

LIST OF FIGURES

LIST OF TABLES

CHAPTER I

BACKGROUND AND INTRODUCTION

A. Background

1. The Vapor Explosion and Fragmentation

> "Once a careless worker poured two tons of molten metal into a chilling pit.....in which there were only a few gallons of water. The resulting explosion hurled a United States Senator, who had come to observe the new miracle (the Bessemer process), across the room and blew Eber Ward out the door and onto a scrap pile." (1)

This rather humorous account describes a vapor explosion that occurred about a hundred years ago in the metals industry. Other more current examples of vapor explosions serve to demonstrate that even today, the vapor explosion is a potential problem to a variety of industries. These include the paper industry, the liquid natural gas industry, the metals industry, and the nuclear industry (1, 2, 3, 4). There is thus considerable incentive to develop an understanding of the mechanism(s) that can produce vapor explosions.

Explosive vaporization of a liquid can occur when it comes into contact with another liquid at a temperature substantially above its boiling point. For such a vapor explosion to occur the rate of vaporization of the liquid must be very high, and simple order of magnitude calcula-

tions indicate that if the usual heat transfer rates are assumed the initial contact area between the two materials must in some cases increase by several order of magnitude in order to account for the observed energy release rates (1). This is the chief reason for the belief held by some that the key to understanding the vapor explosion lies in the mechanism(s) that increase the surface area between the hot and cold materials.

Fragmentation does not necessarily lead to a vapor explosion, however, and there are those who believe that the vapor explosion in some cases actually precedes fragmentation. It should therefore be pointed out that there is not necessarily a one to one correspondence between fragmentation and the vapor explosion. But since it is believed that fragmentation can result in a vapor explosion, and fragmentation at the very least represents a means for dispersing a hot material throughout a coolant (a process that may be of particular importance to the field of reactor safety), the identification of the fragmentation mechanism(s) should receive high priority.

2. Some Proposed Theories of Free Contact Fragmentation

The present paper concerns itself only with the free contact mode of fragmentation, which by definition occurs only where a hot and cold liquid come together at a low

Weber number in the absence of contact with solid boundaries. These restrictions eliminate the alternate modes of fragmentation of hydrodynamic fragmentation, entrapment fragmentation (vaporization of a liquid trapped between a hot liquid and a solid boundary), and the fragmentation due to the Weber number effect (where the ratio of inertial to surface tension forces becomes sufficiently great). These alternative modes of fragmentation are all discussed in detail by Kazimi (5). Additionally, the typical case considered here is the introduction of a mass of the hot, molten material into the cooler liquid, either by dropping or injection. These are the conditions of many fragmentation experiments, and they resemble what could occur in the case of molten UO_2 escaping into the coolant in a nuclear reactor.

One of several plausible theories advanced to explain fragmentation under these restrictions is that of spontaneous nucleation proposed by Fauske (6). Simply stated, it requires that whenever perfect liquid-liquid contact is achieved between the hot and cold liquids, and the interface temperature is at or above the homogeneous nucleation temperature of the cooler liquid, homogeneous nucleation will occur in the cooler liquid and fragmentation of the hot liquid may result. This theory fails to explain the fragmentation that has been shown to occur even when

the interface temperature is below the homogeneous nucleation temperature of the cool liquid (UO_2 and stainless steel in liquid sodium, (7)), but to its credit the spontaneous nucleation theory explains successfully a number of other experimental observations.

Another proposed mechanism for free contact fragmentation that has been given a great deal of attention is the jet penetration theory considered by Board, among others (8, 9). This theory holds that the collapse of a vapor bubble, or the local collapse of a vapor film near the molten material, can lead to a high energy jet of coolant which can penetrate the hot material. If it becomes entrapped within it and subsequently vaporizes, it may cause the hot material to fragment. The details of the collapse induced jet phenomenon are given by Plesset (10).

Numerous other theories have been proposed to describe the experimental observations of fragmentation. In most of these, the major focus is on the identification of a single mechanism capable of describing fragmentation in all cases. More recent thought is leading to the conclusion that there are probably several functioning fragmentation mechanisms. These mechanisms may in fact compete, with each dominating under a different set of conditions.

B. Introduction to the Experiment

1. General Discussion of the Acoustic Cavitation Theory of Fragmentation

The acoustic cavitation theory of fragmentation was originally proposed by Kazimi (5) to explain the free contact fragmentation of hot molten materials suddenly immersed in cool liquids. At least two fundamental requirements must be met for this mechanism to be operative. First, negative pressures must be generated within the molten material of sufficient magnitude to cause cavitation. And second, once the cavitation nuclei have formed they must behave in such a way as to fragment the droplet.

To date, the work at MIT has focused on the mechanism satisfying the first of these requirements. Specifically, a model has been developed to calculate the pressure oscillations in the interior of molten spherical droplets due to sudden immersion in cool liquids. The time dependent pressure in the dynamically growing vapor film was calculated by Kazimi (5). The resultant film pressure is used as a driving function acting at the surface of the molten droplet in the calculations made by Watson (11) in order to determine the resultant pressures in the interior of the droplet. Inasmuch as the data resulting from the present experiment will be used to check the acoustic cavitation theory, it is appropriate to look in more

detail at these calculational models. In the following sections the work of both Kazimi and Watson will be considered briefly, and finally, the expected influence of various dependent variables on the extent of fragmentation will be presented.

Data against which to compare these predictions can be found in the paper by Kazimi (5), as well as in numerous other references (8, 9, 16, 19, 20 and 21).

2. The Calculation of Dynamic Film Growth

Kazimi (5) considered the case of a hot, spherical particle (or droplet) that is instantaneously immersed in a large amount of subcooled liquid. The hot sphere is assumed to be surrounded by a thin film of non-condensible gases at the time of immersion, an assumption introduced both out of mathematical necessity as well as out of a consideration of what would realistically be expected in the case of molten UO_2, with its attendant fission gases, escaping into liquid sodium.

Phenomenologically, the dynamic film growth process can be considered as in Figure 1, which portrays both the initial assumptions and the processes considered in the calculations. The sphere is assumed to be hot enough initially to support film boiling. A portion of the heat conducted away from the sphere goes into vaporizing liquid at the liquid-vapor interface, and consequently the liquid must be displaced away from the sphere to make room for the

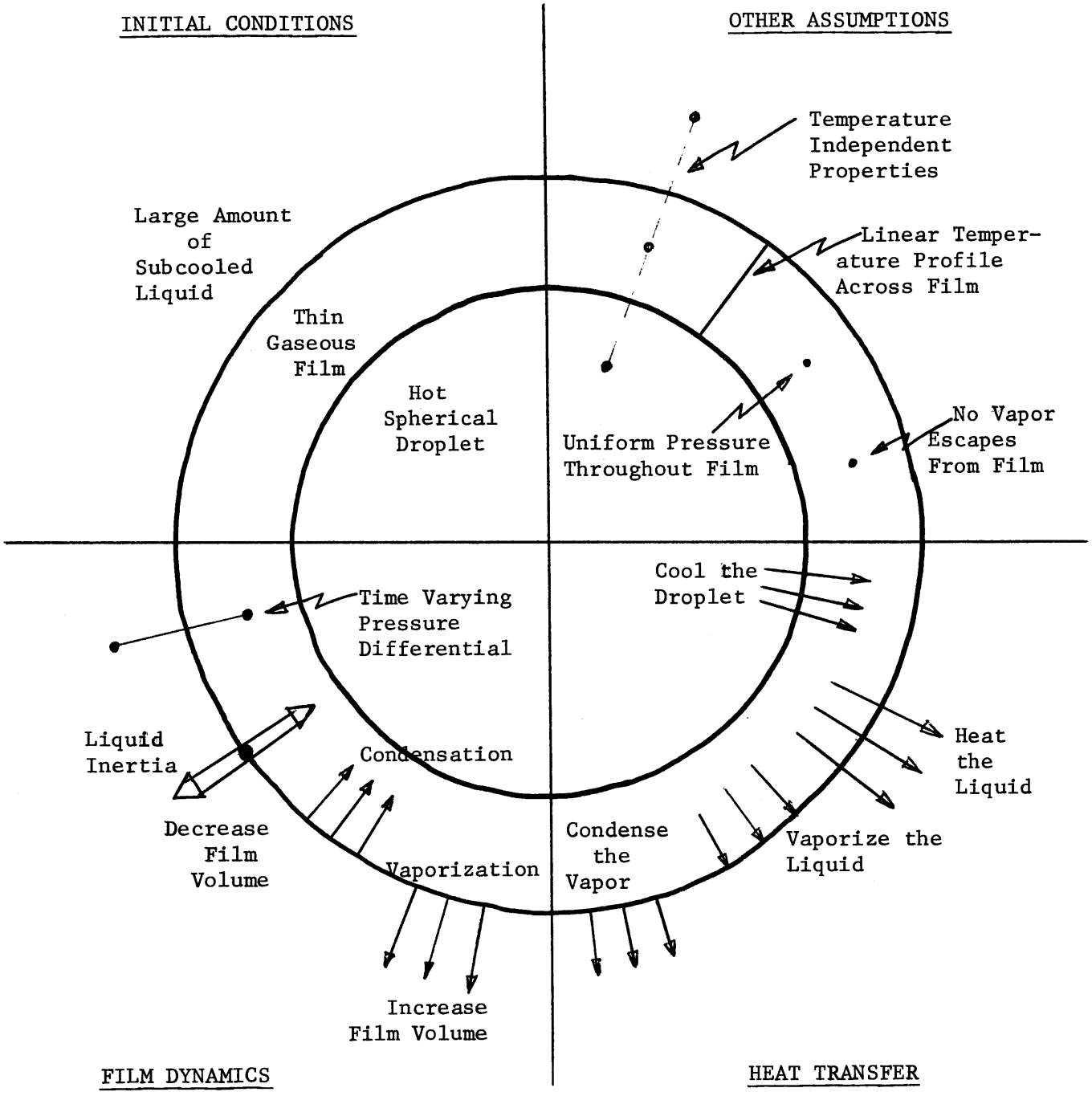

Tab 5/4/74

FIGURE 1

SCHEMATIC REPRESENTATION OF KAZIMI'S MODEL

less dense vapor that is created. The net result is an acceleration of the liquid-vapor interface away from the sphere. The liquid inertia carries the interface beyond the equilibrium point where the pressure in the film exactly equals the pressure in the liquid, and so the liquid is accelerated back toward the droplet. A cyclical process results where the vapor experiences an oscillatory growth accompanied by an oscillating pressure in the vapor film.

Kazimi's model has been used to calculate the time dependent film pressure for a range of conditions and materials. For given droplet and pool materials, the parameters varied are the droplet temperature, droplet radius, pool temperature, and the thickness of the initial film. The result of a typical calculation is shown in Figure 2, which represents the calculated absolute film pressure versus time for a 500°C droplet of molten tin (with a radius of 0.3 cm and an initial film thickness of 10^{-5} cm) suddenly immersed in a pool of water at 20°C. Several features are of interest.

The maximum and minimum pressures, for example, occur on the first cycle and decay thereafter within a clearly defined envelope. The peak pressure of 52 psia occurs at about 1 μsec, and the minimum pressure of 6 psia occurs shortly thereafter. Although still oscillating at 1 msec, the film pressure at this time is close to the ambient pressure.

FIGURE 2

CALCULATED ABSOLUTE FILM PRESSURE VERSUS TIME

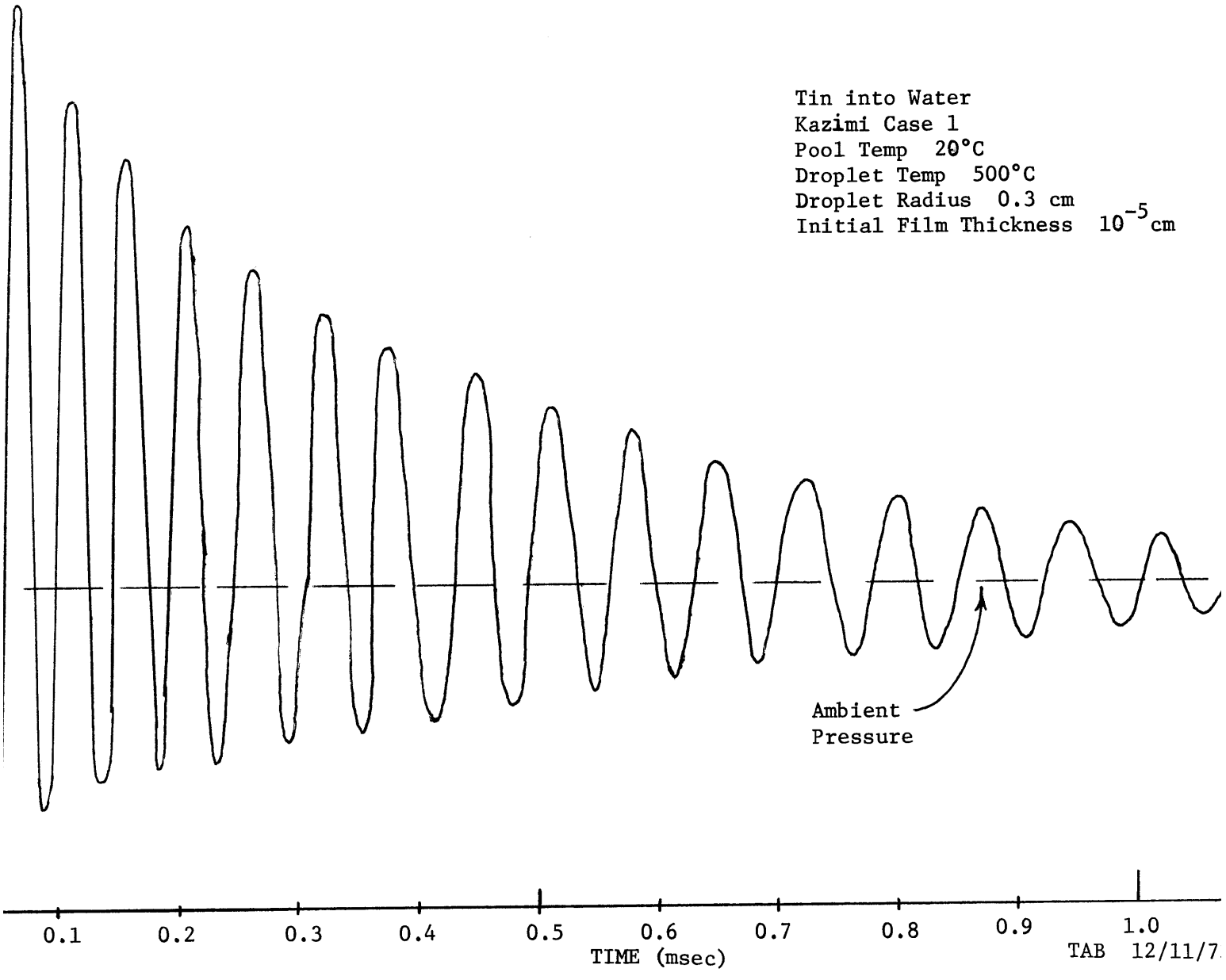

A second feature of interest is the observation that the period of each successive cycle increases with time. The averaged frequency over the time interval from 0 to 0.5 msec is 20,000 Hz, for example, whereas the averaged frequency over the interval 0.5 to 1 msec is only 13,725 Hz. The frequency measured, therefore, would depend on the time at which the measurement was performed.

The calculated effect of three independent variables on the dynamic film behavior are presented in Figures 3 through 5. All calculations assume that the water pool is incompressible and that an initial film of thickness 10^{-5} cm is present. It is clear from Table 1, which summarizes quantitatively the results of these figures, that the effect on film pressure frequency and peak pressure of each of the three variables considered is approximately the same. Specifically, increasing the pool temperature, increasing the initial droplet temperature, and increasing the droplet radius are all calculated to decrease the observed frequency, while increasing the peak film pressure.

FIGURE 3

THE CALCULATED EFFECT OF POOL TEMPERATURE ON VAPOR FILM RESPONSE

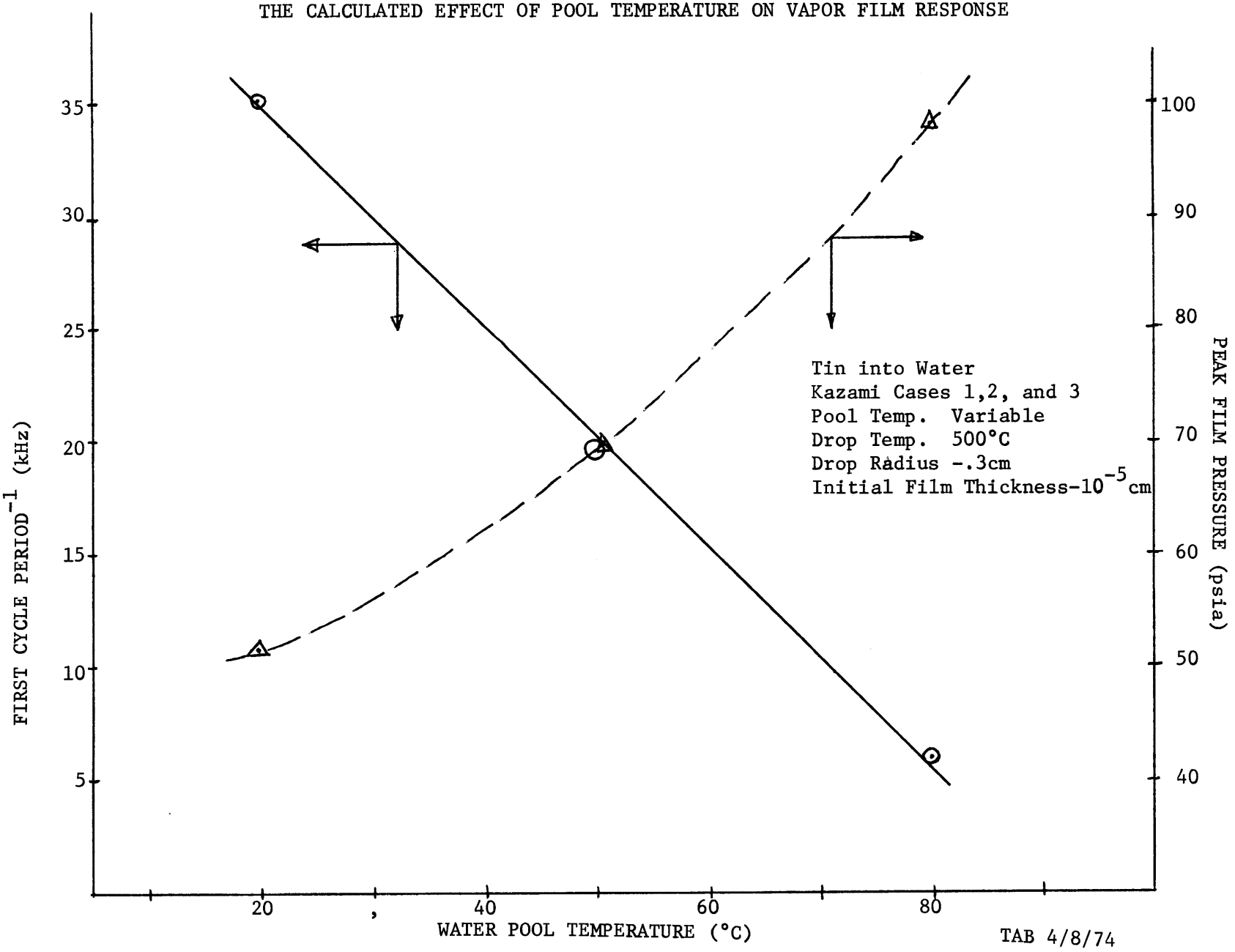

TAB 4/8/74

FIGURE 4

THE CALCULATED EFFECT OF INITIAL DROPLET TEMPERATURE ON VAPOR FILM RESPONSE

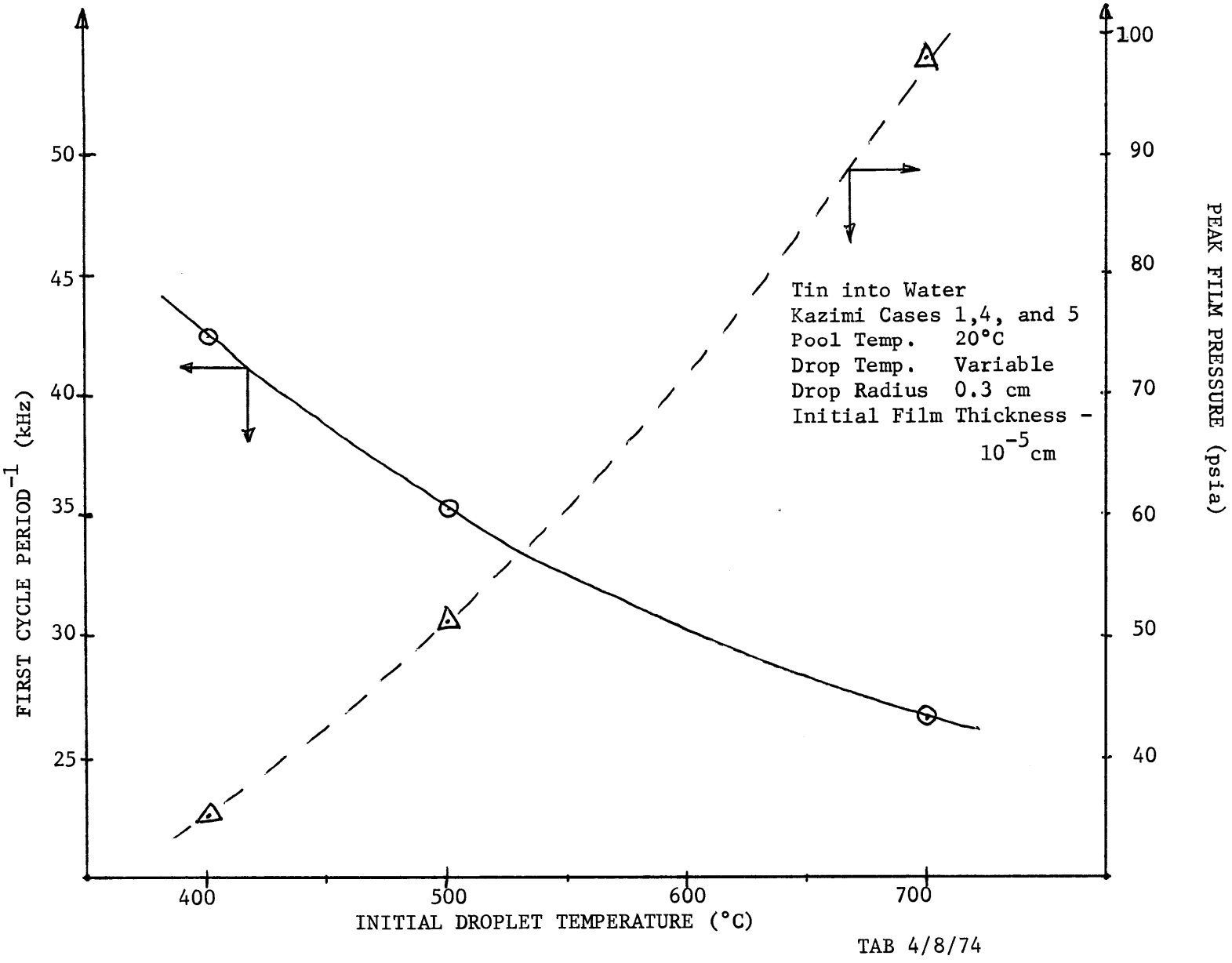

TAB 4/8/74

FIGURE 5

THE CALCULATED EFFECT OF DROPLET RADIUS ON VAPOR FILM RESPONSE

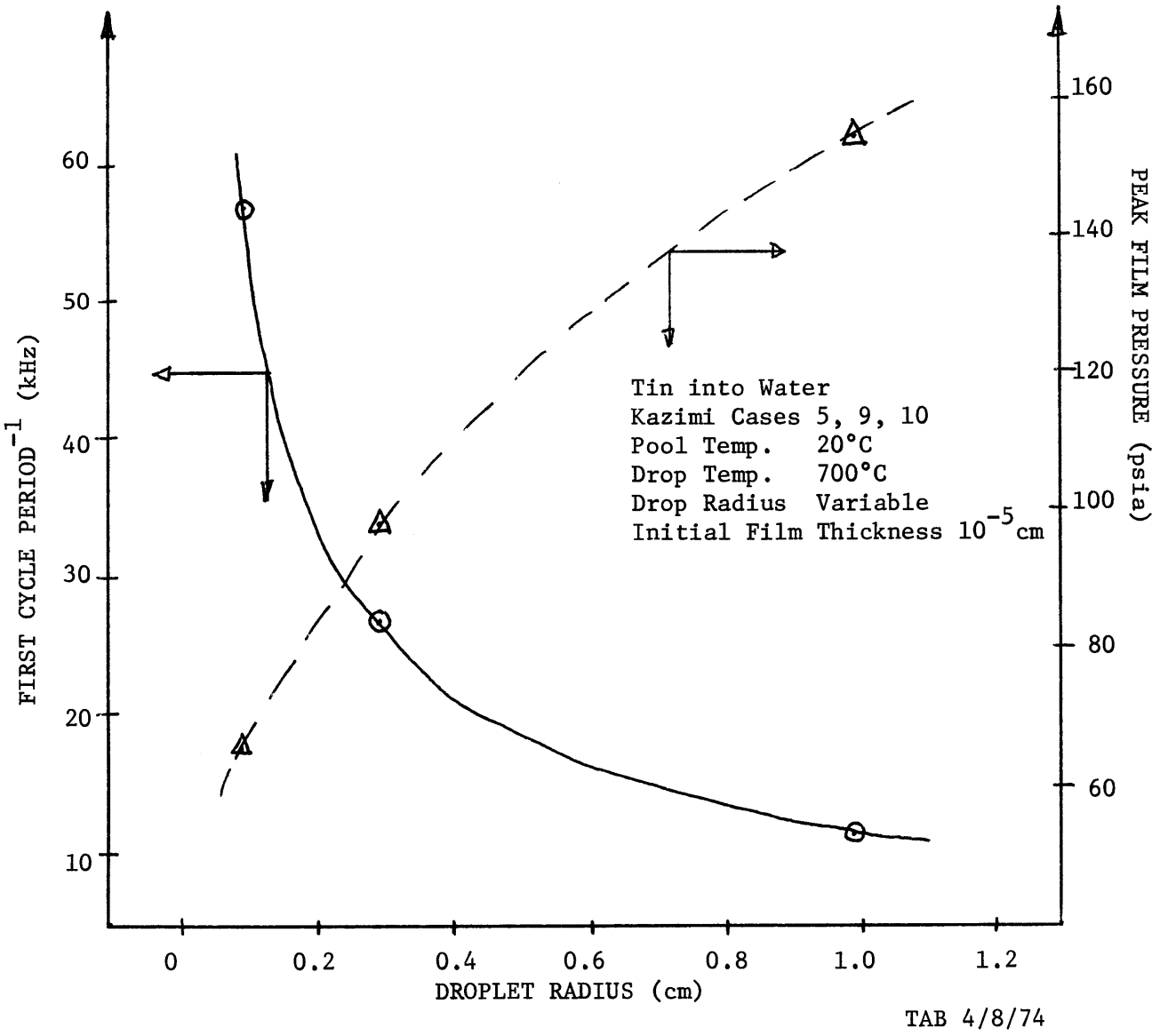

TAB 4/8/74

TABLE 1

THE CALCULATED EFFECT OF THE INDEPENDENT VARIABLES ON

THE FILM PRESSURE FREQUENCY AND THE PEAK FILM PRESSURE

CASE (#)	Key Variable	Pool Temp (°C)	Initial Droplet Temp. (°C)	Droplet Radius (cm)	*(First Cycle Period)$^{-1}$ (sec^{-1})	Peak Film Pressure (psia)
1	Pool Temp.	20	500	0.3	35260	51.5
2		50	500	0.3	19710	69.9
3		80	500	0.3	6120	98.3
4	Droplet Temp.	20	400	0.3	42400	35.6
1		20	500	0.3	35260	51.5
5		20	700	0.3	26870	97.8
9	Droplet Radius	20	700	0.1	56700	65.6
5		20	700	0.3	26870	97.8
10		20	700	1.0	11700	154.9

All cases reported are for:

Tin into H_2O

incompressible liquid (H_2O)

initial film thickness = 10^{-5}cm

*(FIRST CYCLE PERIOD)$^{-1}$ = inverse of the time between the first two maxima in the calculated film pressure

3. Calculation of Pressure Behavior in Interior of Molten Droplet

Watson (11) developed a model for calculating the pressure behavior in the interior of the molten droplet. Beginning with the acoustic wave equation for a compressible viscous fluid, and including the effects of thermal conduction, Watson derived an expression for the pressure in the interior of the sphere due to the oscillating film pressure acting as a driving function at the surface of the droplet. The analytical result is

$$p(r,t) = \int_{-\infty}^{\infty} \frac{a}{r} \frac{\sin kr}{\sin ka} p_{\omega}(a) e^{-i\omega t} d\omega, \quad r \leq a \qquad (1)$$

where a is the molten sphere radius and r is the radius variable ($r \leq a$), k is the wave number, $k = \frac{\omega}{c} - i\varepsilon$, where ε is an artificial convergence parameter, c is the velocity of sound in the molten material, ω is the angular frequency, and $p_{\omega}(a)$ is the Fourier Transform of the surface pressure p(a,t), which is mathematically stated as

$$p(a,t) = \int_{-\infty}^{\infty} p_{\omega}(a) e^{-i\omega t} d\omega \quad . \qquad (2)$$

Watson solved equation (1) numerically on the computer using the Cooley Tukey Fast Fourier Transform subroutine FOURT. The results for the cases of present interest are shown in Figures 6 through 8. Plotted in these figures is the pressure behavior at the center of the molten sphere as a function of pool temperature (Figure 6), initial droplet temperature (Figure 7), and droplet radius (Figure 8). Of primary interest here are the time scale of the interior oscillations and the magnitude and duration of the negative pressure swings. The maximum negative pressures, ranging up to about -400 psia, occur within the first 20 μsec. Increasing the pool temperature, droplet temperature and droplet radius all have the same effect of increasing the magnitude of the maximum negative pressure. Additionally, as each of the three variables is increased the duration of time that the droplet center experiences a negative pressure is also increased. This may have some bearing on the subsequent behavior of cavitation bubbles.

The theoretical negative pressures required for acoustic cavitation are known to be on the order of several thousands of atmospheres (12). Under even the most carefully controlled experimental conditions, however, only fractions of these pressures have been reached. For H_2O at 20°C, for example, theory predicts a cavitation pressure of -1,039 atm, whereas the experimental maximum is only

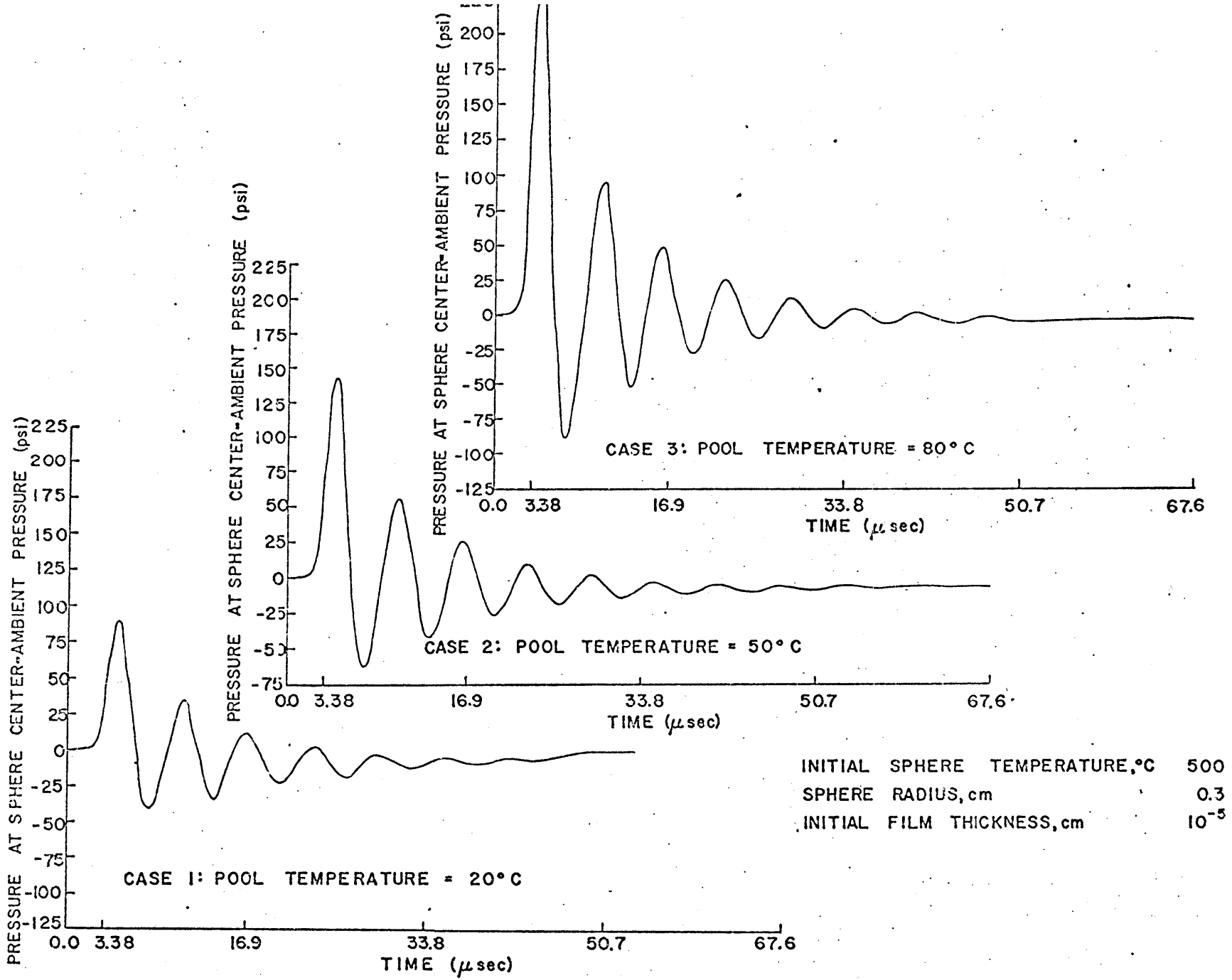

FIGURE 6

THE CALCULATED EFFECT OF POOL TEMPERATURE ON THE PRESSURE AT THE SPHERE CENTER

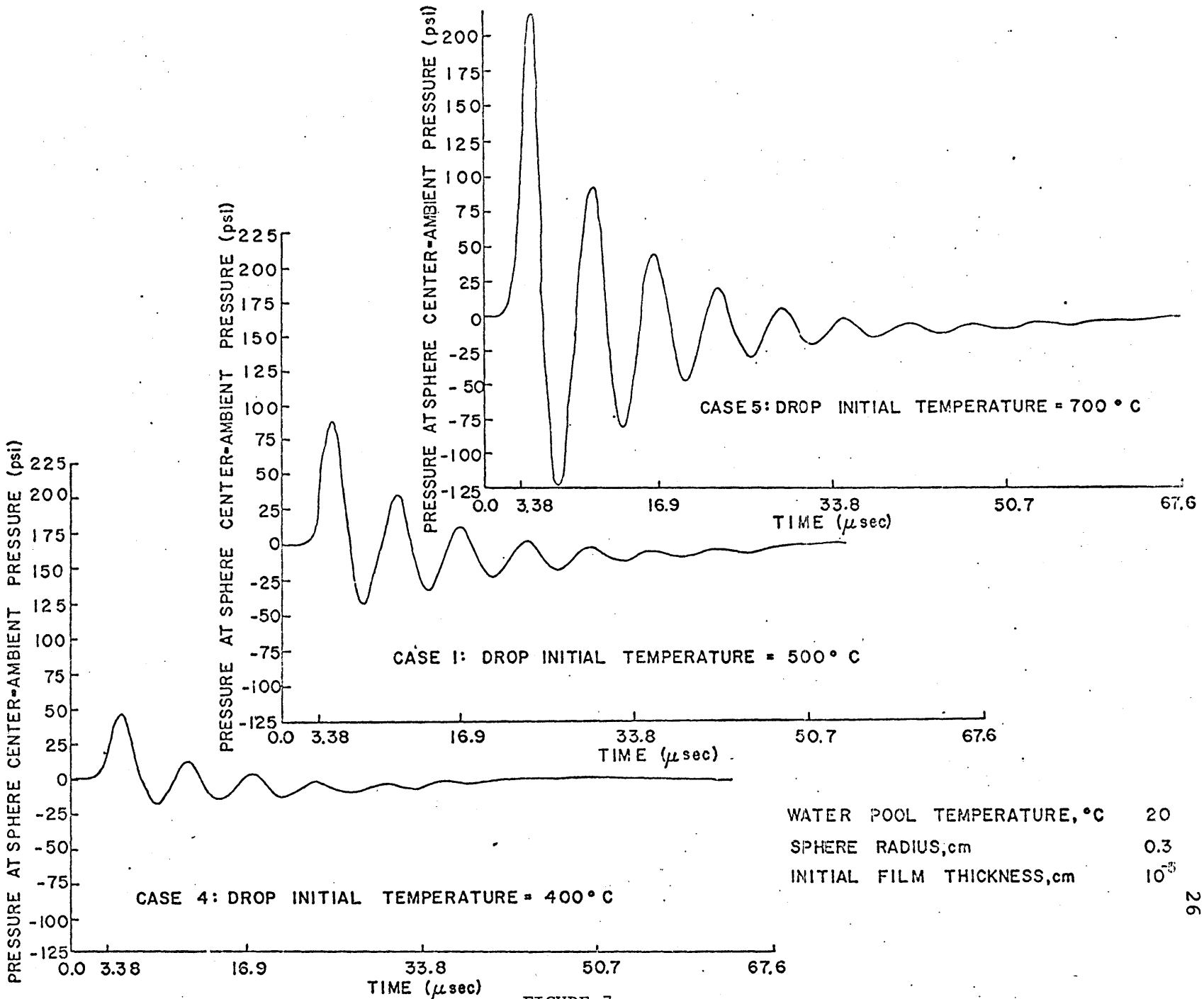

FIGURE 7

THE CALCULATED EFFECT OF INITIAL DROPLET TEMPERATURE ON THE PRESSURE AT THE SHPERE CENTER

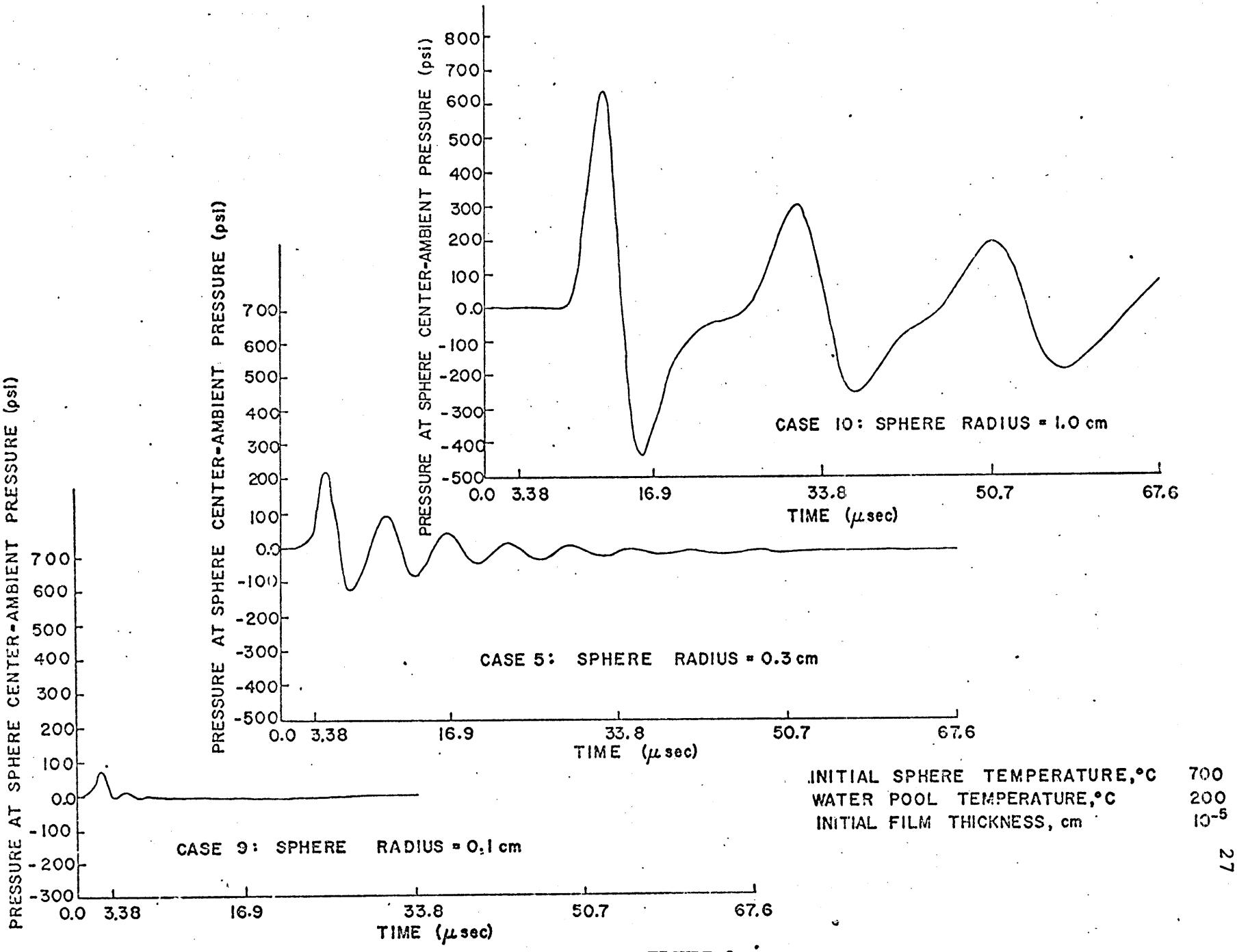

FIGURE 8

THE CALCULATED EFFECT OF DROPLET RADIUS ON THE PRESSURE AT THE SHPERE CENTER

-281 atm (13). For Hg at 300°C, the values are -11,900 atm and -460 atm, respectively. Thus it appears reasonable to assume that although the theoretical cavitation pressures for many materials are far greater in magnitude than those calculated to occur by Watson, cavitation may nonetheless occur at the smaller pressures due to the presence of impurities. One can then postulate that in the cases considered by Kazimi and Watson, the first of the two requirements of the acoustic cavitation theory of fragmentation may be met. Work is currently planned to analyze in detail the means by which the cavitation nuclei, once formed, can fragment the droplet.

4. The Pressure Wave in the Coolant

The pressure oscillation in the vapor film acts as a source of acoustic waves in the coolant pool. Inasmuch as the measured coolant pool pressure history will later be compared to Kazimi's film pressure calculations, it is necessary to be able to analytically relate the measured pool pressure to the calculated film pressure.

An expression for the 'exterior' pressure wave can be derived in a number of ways. A particularly instructive way to do so is to begin with a derivation made by Watson (11) that parallels his interior solution. This will provide an additional check on the validity of his

approach. Watson (14) has shown that the exterior pressure wave is described by the relation

$$p(r,t) = \frac{a}{r} \int_{-\infty}^{\infty} e^{ik(r-a)} \; p_{\omega}(a) e^{-i\omega t} \, d\omega$$

$$\text{for } r > (a + \delta) \qquad (3)$$

where the terms are as previously defined except for c, which is now the speed of sound in the coolant, and δ is the thickness of the film. This equation is somewhat unmanageable in its present form but fortunately yields readily to mathematical simplification. First, one obtains

$$p(r,t) = \frac{a}{r} e^{\varepsilon(r-a)} \int_{-\infty}^{\infty} p_{\omega}(a) e^{-i\omega(t-\frac{r-a}{c})} d\omega \qquad (4)$$

by making use of the fact that $k = \frac{\omega}{c} - i\varepsilon$. Writing the series expansion of $e^{\varepsilon(r-a)}$, the relation

$$e^{\varepsilon(r-a)} = 1 + \frac{\varepsilon(r-a)}{1\,!} + \frac{\varepsilon(r-a)^2}{2\,!} + \ldots \simeq 1 \qquad (5)$$

results since ε is small (about 10^{-4} cm). Furthermore, since $(\frac{r-a}{c})$ is simply the time required for a wave moving at speed c to travel a distance (r-a), it becomes clear that this term has the effect of shifting the exterior solution in time by a value constant for fixed r. Letting

$$t' = t - (\frac{r-a}{c}) = t - \Delta t \tag{6}$$

and making use of the approximation in equation (5), equation (3) simplifies to

$$p(r,t) \approx \frac{a}{r} \int_{-\infty}^{\infty} p_{\omega}(a) e^{-i\omega t'} \, d\omega \quad . \tag{7}$$

Furthermore, by making use of the fact that $p_{\omega}(a)$ is the Fourier Transform of p(a,t) (Eq. 2), one gets the much simplified relation

$$p(r,t) \approx \frac{a}{r} p(a,t') \quad . \tag{8}$$

This equation relates the pressure at time t in the coolant (at a point r > a) to the film pressure at a previous time t', and assumes that the film thickness is

small compared to the droplet radius. Thus the pressure behavior in the coolant pool is qualitatively the same as that in the film, with the only difference that it is reduced in magnitude by the factor a/r and is shifted in time by an amount $\frac{r-a}{c}$.

It is instructive at this point to discuss the predicted (a/r) dependence in the general context of a radiating spherical source. For a spherical source radiating light, for example, it is a well known fact that the intensity falls off as the inverse of the distance squared, $(a/r)^2$. This is also true of the intensity of an acoustic wave (15, pg. 240). The acoustic intensity, however, is proportional to the square of the pressure, and so the pressure should vary as the square root of the intensity , or as a/r. This is in agreement with the result obtained.

5. The Experimental Goal

The motivation for the series of dropping experiments begun with the present work is to experimentally investigate the acoustic cavitation theory of fragmentation. Since the film pressure oscillation that drives the droplet interior pressure also sends acoustic waves into the coolant, recording the coolant pressure pulse and comparing it to the calculated behavior (given by Eq. 8) will give a good indication of whether or not the film pressure behavior

is being accurately calculated by the Kazimi model. Since it has been shown that for any given observation point in the coolant the measured pressure behavior should qualitatively match the calculated film pressure, such a comparison will be quite straight forward. The present experiment is aimed at providing the experimental data necessary for this comparison.

The scope of the work reported here is to determine, for a fixed material and droplet radius (tin and 0.3 cm, respectively) the effect of varying the initial droplet temperature and the water pool temperature on the film pressure behavior. Further experiments are planned in which the droplet material and radius will be varied.

CHAPTER II

EXPERIMENTAL APPARATUS

A successful experiment is favored by conditions which match, as closely as possible, the conditions assumed in the calculations. Thus the experiment requires that a spherical, molten metal droplet of known size and temperature be suddenly immersed in a large amount of coolant of known temperature. Additional constraints are that the molten droplet must enter the coolant at a sufficiently low Weber number, and also that the coolant must be acoustically infinite. Furthermore, means must be provided for recording and analyzing the pressure pulse in the coolant. This section will describe the apparatus used to meet the above requirements.

A. Production of Molten Metal Droplets

A small amount of the drop material is placed in the crucible of the "automated dropping mechanism" shown in Figure 9. The crucible is then lowered into the vertically oriented core of a Hoskins 5 kw electric furnace which is positioned several inches above the coolant pool surface. The metal temperature is measured by a chromel-alumel thermocouple in conjunction with a 1500°F thermocouple readout (a Pyro indicating pyrometer). When the metal reaches the proper temperature, the crucible is lowered to a position just above the coolant pool surface and the

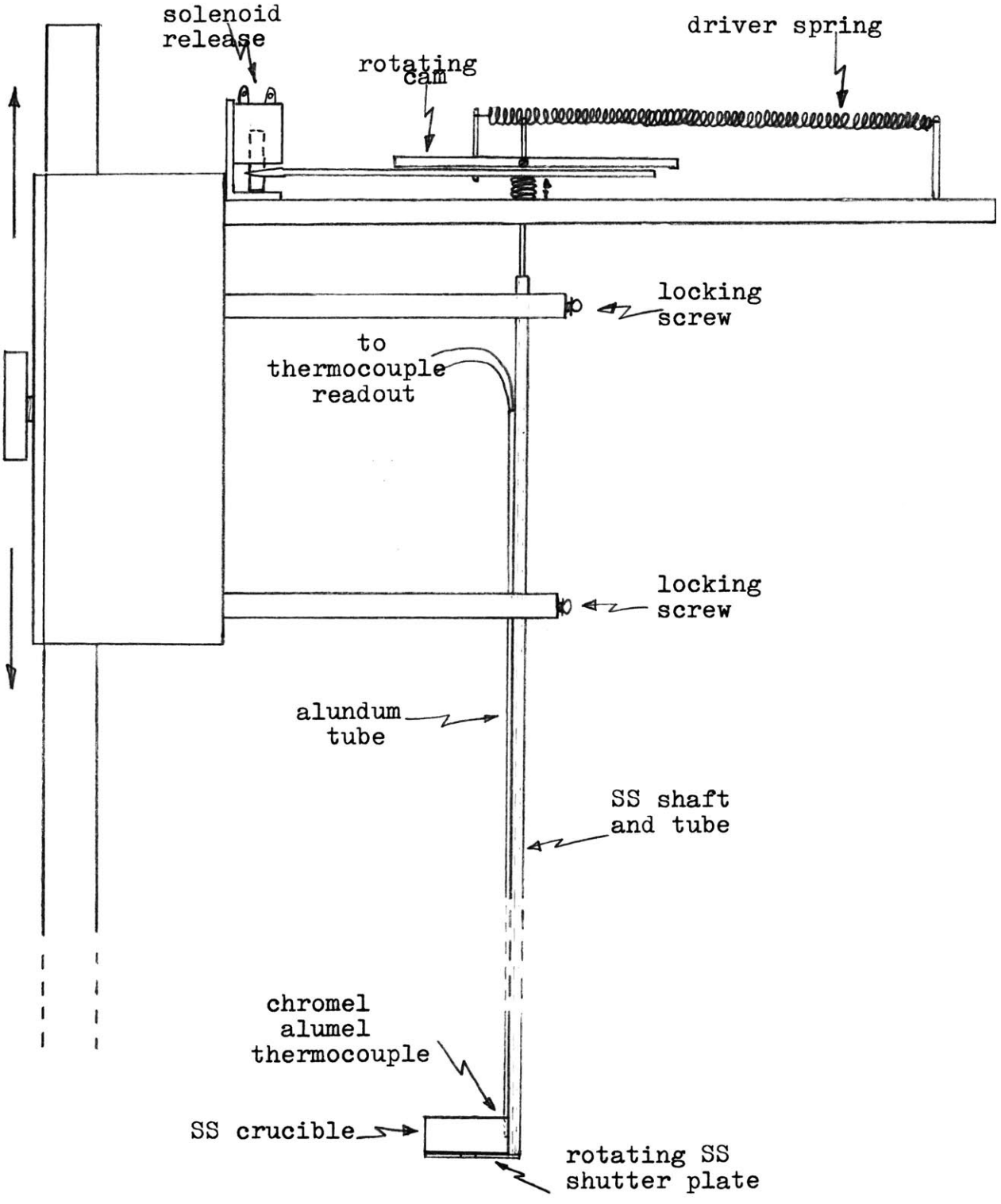

FIGURE 9

Automated Dropping Mechanism

drop is produced by pressing a button which activates the solenoid release. This allows the driver spring to turn the rotating cam, and together with it the rotating shutter plate beneath the crucible. A hole in the shutter plate lines up with a hole in the base of the crucible just long enough for a single drop to squeeze through.

This method of producing the molten droplets has several attractive features. First, this scheme is extremely reliable - once the apparatus is properly adjusted, single droplets result almost every time. Secondly, droplets of a given size can be consistently produced simply by loading the crucible with the appropriate initial mass. This can readily be seen from Figure 10, which is a plot of the mass of the droplet produced versus the initial crucible loading mass (for tin at 800°F). The droplet mass is a linear function of the loading mass over this range. It is apparent from this figure that in order to produce a molten tin droplet of 0.3 cm radius, the crucible must initially contain about 4.5 gm of tin. The effect of increasing the droplet temperature can be seen from Table 2 to have a negligible effect on the size of the droplets produced.

McCracken (16) found that the presence of oxide on the metal surfaces had a pronounced effect on the fragmentation behavior, and consequently he took the trouble to

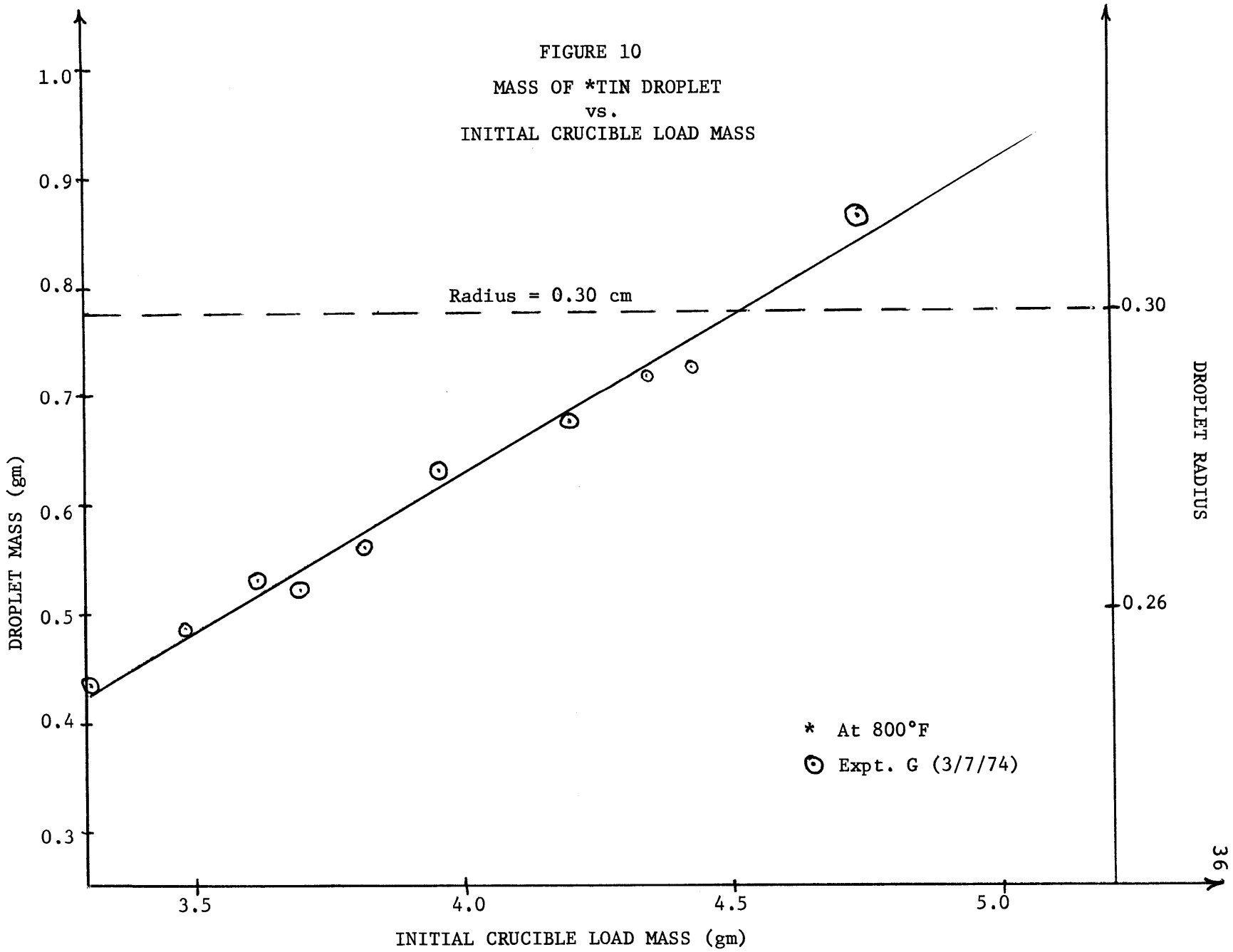
FIGURE 10
MASS OF *TIN DROPLET
vs.
INITIAL CRUCIBLE LOAD MASS
1.0
0.9
0.8
0.7
0.6
0.5
0.4
0.3
DROPLET MASS (gm)
Radius = 0.30 cm
0.30
0.26
DROPLET RADIUS
* At 800°F
Expt. G (3/7/74)
3.5
4.0
4.5
5.0
INITIAL CRUCIBLE LOAD MASS (gm)

TABLE 2

THE EFFECT OF INITIAL DROPLET TEMPERATURE

ON DROPLET RADIUS

Case No.	Pool Temp.	Initial Droplet Temp.	Fragment Mass	Density (Ref. 17)	Average Radius
#	(°C)	(°C)	(gm)	(gm/cm^3)	(cm)
1	21	300	0.844		
2	21	300	0.872	6.84	0.309
3	21	300	0.826		
34	40	500	0.842	6.78	0.308
35	40	500	0.815		
36	40	600	1.080	6.70	0.337
38	39.5	600	1.080		

scrape away the oxide before each trial. In the present experiment, this problem is avoided. The droplets are drawn off from the bottom of the crucible and are consequently oxide free, at least initially. The only oxide present will be that which forms during the fall of the droplet to the coolant pool surface. For tin, this is minimal. This method works well in a normal atmosphere of air up to tin temperatures of 700°C. At temperatures greater than 700°C, oxide formation on the crucible surface prevent a droplet from being released.

Also important in the context of droplet production is the shape of the droplets, insofar as the entrance geometry may have some influence on the subsequent phenomenon. Numerous still photographs taken of tin droplets falling through air showed that the droplets consistently had the same shape - that of a nearly spherical teardrop. There was an observed tendency for the droplet to rotate slightly during its fall from the crucible to the coolant surface, but this appeared to occur in a consistent fashion so no variability due to this is foreseen.

The effect on the pressure behavior of varying the droplet radius is of primary interest to the acoustic cavitation theory, since the theory predicts a clear trend of pressure behavior as a function of droplet

radius (see Figures 5 and 8). The range of radii achievable with the present crucible/shutter plate combination is quite limited - from about 0.26 cm to 0.31 cm. The dropping mechanism was designed with a removable crucible/shutter plate, however, to permit larger (or smaller) droplets to be produced merely by inserting a new crucible/shutter plate combination in the holding device. Fine tuning of the droplet radius produced by any particular crucible/shutter plate combination can easily be achieved by varying both the initial load mass and the tension provided by the driver spring.

B. Pressure Measurement and the Associated Electronics

The coolant pressure wave is detected by a PCB Piezotronics model 102A12 pressure transducer. This is a voltage mode device for measuring dynamic pressure that has a linear frequency response to frequencies greater than 100 kHz. Its relatively high sensitivity (about 23.5 millivolts per psi) and ability to withstand moisture and temperatures up to 250°F make it suited to the purposes of this experiment. The rise time of the transducer is 1 μsec.

The pressure signal from the transducer is recorded in analog form on a Ballantine model 7050A Electronic Signal Recorder. This unit records signals of 20 msec duration to frequencies greater than 100 kHz. The unique

feature of this recorder is that the signal is recorded directly onto a small loop of magnetic tape, thereby allowing analysis of the recordings to be performed at any later time by playing back the recorded tape through the recorder.

The drawback with the Ballantine recorder is that it can only record for a maximum duration of 20 msec. Data of other dropping experiments of tin into water have shown that interaction times significantly longer than 20 msec are to be expected for some conditions. Buchanan and Dullforce, for example, measured dwell times* of up to 150 msec for tin dropped into water at 34°C (8). These long dwell times lead to the difficulty that in these cases only a small fraction of the interaction can be recorded on tape. This potential problem is circumvented in the present experiments by photographing an oscilloscope trace of the entire signal while at the same time recording only a 20 msec 'window' of the pressure pulse on the signal recorder. This method allows detailed analysis of the 20 msec recording while also retaining information of the longer term behavior.

---

* The 'dwell time' is defined as the time interval between droplet immersion and the onset of fragmentation.

A schematic of the electronic circuits used is shown in Figure 11, which illustrates that the pulse from an optical trigger circuit is used both to trigger the oscilloscope trace (Tektronics Type 585 oscilloscope) and also to initiate the time delayed triggering of the signal recorder. The time delay is continuously variable to well over 1 second, thus providing the capability for positioning the tape loop recording window at any desired moment of the interaction.

Analysis of the signals is performed in two ways. The pressure signal frequency and amplitude is determined by playing the recorded signal into an oscilloscope. Areas of the recording that are found to be of particular interest can be expanded on the oscilloscope screen and examined in great detail.

Spectrum analysis was felt to be a useful backup to the visual oscilloscope analysis not only because of its mechanical objectivity, but also because spectrum analysis can resolve frequency components that are not readily detected by the oscilloscope method. In the present experiment, the spectrum analysis is performed using a Nelson-Ross model PSA-032 spectrum analyzer. This particular analyzer was chosen in order to span the entire frequency range of interest, and covers the range from 35 Hz to 100kHz. Its resolution varies from 35 Hz to 250 Hz, depending upon the frequency range being scanned.

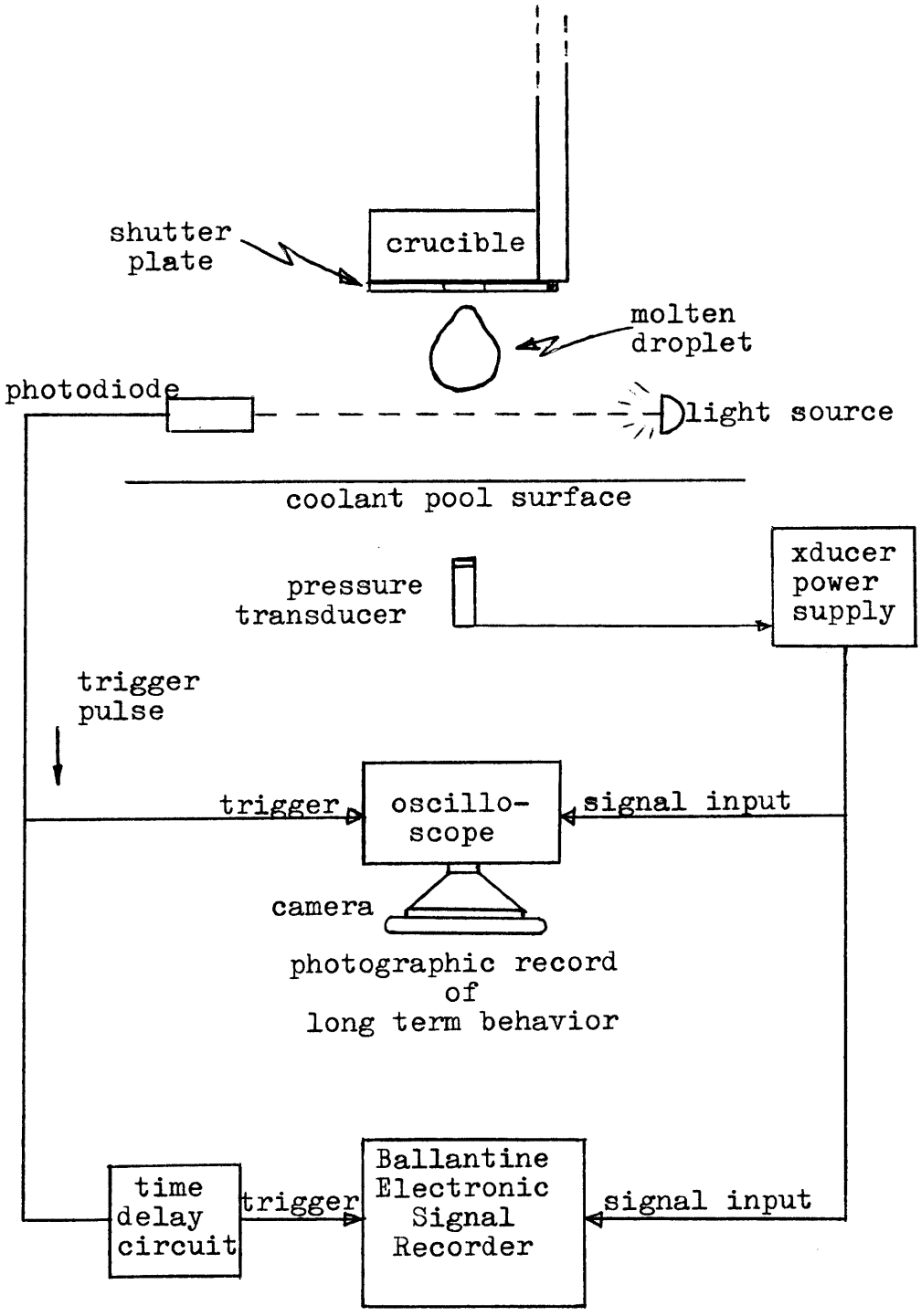

FIGURE 11

Schematic of Pressure Recording Circuit

C. The Coolant Pool and High Speed Photographic Equipment

It was decided to take high speed motion pictures of the interaction phenomenon while at the same time recording the pressure history, thereby providing the most useful information for any given data point. For a good pressure recording a large tank is desired so that the problem of interference by reflected waves is minimized. Good high speed motion pictures require a small enough tank to allow for sufficient illumination. The choice of the tank size, therefore, requires that a trade-off be made between two factors of importance.

The tank used for the present experiment, shown in Figure 12, is believed to represent a reasonable compromise. It is a commercially available O'Dell aquarium, made of 3/8" plate glass. It is hexagonal in horizontal cross section, with dimensions of 18" across by 24-1/4" deep. There is clearly a limit to the maximum pressures this tank is capable of withstanding, but since the thermal energy available in the small tin droplets used in the present experiment is so small - less than 70 calories for a 0.3 cm radius tin droplet at 1100°C - this is not presently a problem. The use of larger droplets, with the attendant potential for larger pressure generation, may require the use of a thicker walled tank.

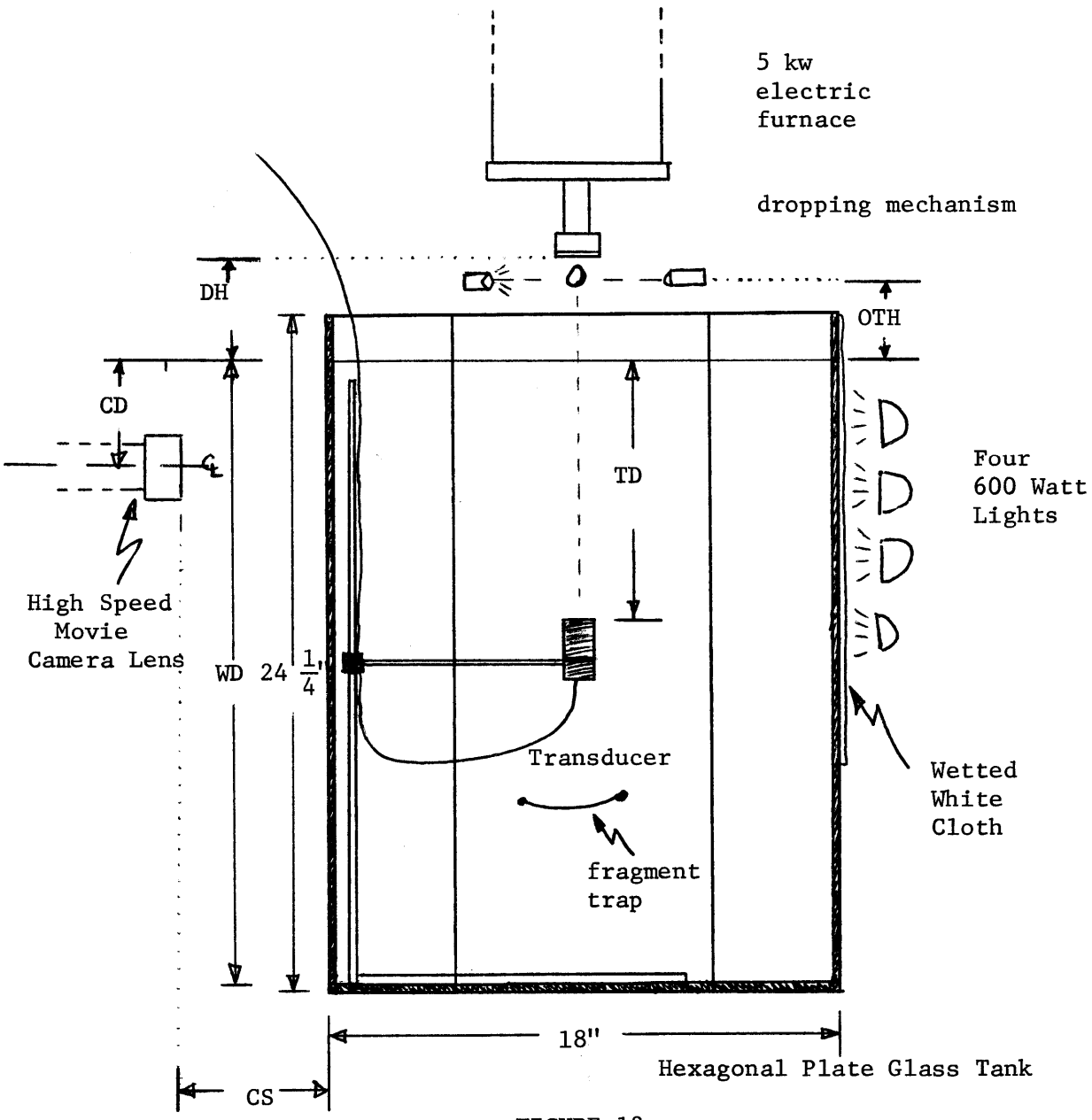

FIGURE 12

SPATIAL ARRANGEMENT OF APPARATUS

The spatial arrangement of the dropping mechanism, tank and photographic equipment is also shown in Figure 12. The 400' Hycam high speed movie camera, capable of photographing at speeds up to about 10,000 fps, is oriented so as to be viewing the illuminated back wall of the tank (backlighting was used). Relatively uniform illumination of the back wall is achieved by shining four Colortram 'Mini-Pro' 600 watt lights on a wetted sheet of white cloth that has been pressed up against the tank from the outside.

The water pool temperature is controlled through the use of three immersion heaters. Two are identical thermostatically controlled heaters that were used to hold the pool temperature constant at a particular temperature, and delivered 200 watts each. The main heater is a 1000 watt immersion heater controlled by a variac. This combination of heaters was found to be satisfactory to temperatures of well over 60°C, but required that the pool be well stirred before any given run to ensure that the entire pool was at a uniform temperature.

Also shown in Figure 12 is the 'fragment trap', or means for collecting the fragmentation residue for any given run. The fragment trap is a large cloth pouch stretched over a wire frame which was suspended beneath the pressure transducer.

D. Pressure Transducer Orientation

The possibility exists for orienting the transducer such that the sensitive face is either in a horizontal or in a vertical plane. The horizontal orientation shown in Figure 12 was chosen for this initial set of experiments in order to minimize the problems associated with the directional characteristics of the transducer. By orienting the transducer such that the molten metal droplets fall toward the recording face, instead of at a right angle by it, the only variable affecting the recorded pressure amplitude is the distance to the transducer. So long as the transducer is positioned deep enough to allow the phenomenon to occur before being impacted by the falling droplet, the entire interaction can be recorded in this manner. A correction can be made to the recorded pressure amplitude to account for the varying distance from the droplet to the transducer.

CHAPTER III

THE EXPERIMENT

A. Procedure

The procedure used in the experiment is presented below in two sections: That which is of a general preparatory nature done prior to the taking of data, and the procedure used at the actual time of the experiment.

Prior to Taking of Data:

1. Carefully position tank and transducer below the dropping mechanism and fill clean tank with fresh distilled water.
2. Record geometry parameters as defined in Figure 12.
3. Check functioning of electronics, paying particular attention to the triggering of the units. Clean the signal recorder heads if required.
4. Clean and check functioning of automated dropping mechanism, making sure both crucible and thermocouple are free of debris, and also that all screws and nuts on the mechanism are tightly fastened.
5. Set polaroid camera and long term oscilloscope to appropriate settings.

6. Determine appropriate delay time for triggering of the electronic signal recorder.
7. Prepare sufficient quantity of tin slugs of appropriate mass for use as crucible loads. A fresh slug of 4.6 gm is used to produce each droplet.

For Each Data Point:

1. Record:
   a) Crucible load mass
   b) Pool temperature (use mercury thermometer)
   c) Initial drop temperature
   d) Signal recorder delay time
   e) Oscilloscope parameters (vertical sensitivity and time base settings)
2. Prime recorder, camera and crucible shutter plate.
3. Inspect transducer face and clean, if necessary.
4. Stir pool to eliminate thermal stratification. Allow pool to quiesce.
5. Position clean fragment trap beneath transducer.

6. Load crucible, lower into furnace core and heat tin to desired temperature (a few degrees above drop temperature).
7. Lower crucible to the dropping position (lowest stop).
8. Turn on lights if high speed motion picture being taken.
9. Start high speed motion picture camera and press solenoid release button when the tin is air cooled to the desired temperature.
10. Raise crucible out of furnace core. Turn off lights if motion picture being taken.
11. Record impression of sound of interaction using code defined in Table 3.
12. Empty and clean crucible before remaining tin solidifies.
13. Remove fragment trap, save residue, and record visual characterization of residue using code defined in Table 4.
14. File tape and polaroid picture for later analysis.
15. Record any noteworthy comments about the run (i.e. errors in procedure, equipment malfunctions, etc.).

TABLE 3

DEFINITIONS OF CODE USED TO CHARACTERIZE THE SOUND OF THE INTERACTION

CODE	DESCRIPTION
NS	No sound discernible
HNP	Hissing, No Pop
SP	Slight Pop
LP	Loud Pop

TABLE 4

DEFINITION OF CODE USED TO CHARACTERIZE THE FRAGMENTATION RESIDUE APPEARANCE

CODE	DESCRIPTION
S	Solid (no evidence of any Fragmentation)
H	Hollow shell
SSF	Largely solid, with slight fragmentation
MF	Moderately fragmented (about 1/2 solid)
TF	Totally fragmented (no large, solid piece)

B. Data

The chemical composition of the tin used in the experiment is presented in Table 5, which shows that the tin was originally 99.9% pure. The handling of the tin required to prepare the crucible loads of the desired mass was felt to have a minimal effect on the tin purity. No chemical analysis results of the distilled water were available.

The data were taken on two separate days. On May 14, the clean tank was filled with fresh, distilled water from 5 gallon poly-bottles, and measurements were taken for a fixed pool temperature of 21°C, with the initial droplet temperature being varied from 300°C to 800°C. Usable data were obtained only up to 700°C since severe oxidation of the surface of the tin in the crucible at 800°C produced an oxide crust that didn't allow a droplet to fall. This posed no problem at the lower droplet temperatures.

The laboratory data recorded on May 14 is presented in Table 5. Although no quantitative information regarding the nature of the interaction is given, the data given are useful in defining the initial conditions, giving the instrument settings, and qualitatively describing both the interaction and

TABLE 5

CHEMICAL COMPOSITION OF *TIN USED

IN DROPPING EXPERIMENTS

Tin (Sn)	99.9%
Nonvolatile with Hydrobromic Acid and Bromine	.02%
Antimony (Sb)	.02%
Arsenic (As)	.00002%
Copper (Cu)	.001%
Iron (Fe)	.004%
Lead (Pb)	.003%
Zinc (Zn)	.0002%

*Reagent grade purchased in stick form

TABLE 6

LABORATORY DATA FOR DROPPING OF TIN INTO $^{+}$DISTILLED WATER
(INITIAL DROPLET TEMPERATURE VARIED)

Drop No.	Temp Initial Droplet Temp.	Temp Pool Temp.	Mass Load Mass	Geometry 1 WD	Geometry 1 DH	Geometry 1 TD	Signal Recorder Recorder Sensitivity	Signal Recorder Recorder Delay Time	Oscilloscope Photos Time Base	Oscilloscope Photos Vertical Sensitivity
(#)	(°C)	(°C)	(gm)	(in)	(in)	(in)	(mv/cm)	(msec)	(msec/cm)	(mv/cm)
1	300	21	4.622	$21\frac{1}{2}$	$2\frac{3}{16}$	$2\frac{3}{16}$	4	35	10	50
2	300	21	4.637	"	"	"	4	35	10	50
3	300	21	4.595	"	"	"	4	35	10	50
4	400	21	4.597	"	"	"	4	35	10	50
5	400	21	4.617	"	"	"	4	35	10	50
6	400	21	4.614	"	"	"	4	35	10	5
7	500	21	4.609	"	"	"	4	35	5	2.5
8	500	21	4.633	"	"	"	4	35	10	2.5
9	500	21	4.629	"	"	"	4	35	20	2.5
10	500	21	4.597	"	"	"	4	35	20	5
11	500	21	4.637	"	"	"	4	40	20	5
12	600	21	4.605	"	"	$4\frac{1}{4}$	4	40	20	5
13	600	21	4.591	"	"	"	10	50	20	5
14	700	21	4.602	"	"	"	10	40	20	5
15	700	21	4.637	"	"	"	10	40	20	50
16	700	21	4.617	"	"	"	10	40	20	10
17	800	21	4.624	"	"	"	10	40	20	10
18	700	21	4.574	"	"	"	10	70	20	10
19	600	21	4.630	"	"	"	4	50	20	10
20	400	21	4.590	"	"	"	4	35	10	5
21	500	21	4.608	"	"	"	4	35	10	2.5

TABLE 6 CONTINUED

Drop No.	Good Tape	Good Oscilloscope Photo	Results [2]Visual	[3]Audio	Comments	High Speed Movie Taken
#	?	?				?(speed)
1	✓	-	H	SP		-
2	✓	-	H	HNP		-
3	✓	-	H	HNP		-
4	✓	-	SSF	SP		-
5	✓	-	SSF	SP		-
6	✓	-	SSF	SP		-
7	✓	-	TF	LP	Recorder didn't trigger	-
8	✓	✓	TF	LP	Recorder didn't trigger	-
9	✓	✓	TF	LP		-
10	✓	✓	SSF	HNP		-
11	✓	✓	TF	LP		-
12	✓	✓	TF	LP		-
13	✓	✓	TF	LP		-
14	-	✓	TF	LP	Recorder didn't trigger	-
15	✓	✓	TF	LP		-
16	-	-	TF	LP	Recorder didn't trigger	-
17	-	-	-	-	Oxide No Droplet	-
18	-	✓	TF	LP	Recorder didn't trigger	✓(3000 fps)
19	-	✓	TF	LP	Recorder didn't trigger	✓(3000 fps)
20	-	✓	H	NS	Recorder didn't trigger	✓(3000 fps)
21	-	✓	TF	LP	Recorder didn't trigger	✓(3000 fps)

[1]See Figure 12 [2]See Table 4 [3]See Table 3

[+]Fresh distilled water. Same water used for all points

the nature of the data obtained for future analysis. Triggering problems with the Ballantine signal recorder resulted in only 12 useful tape records out of 21 runs. No photos of the oscilloscope trace were obtained for the first seven (low temperature) runs due to problems with the photograph settings. This was remedied for the later runs.

A replacement signal recorder was obtained and used in the experiment on May 16. Since on the previous day no tape records had been obtained that captured the fragmentation at a droplet temperature of 700°C, the first few runs were made at a fixed ambient pool temperature of 23°C and a droplet temperature of 700°C in order to obtain this recording. Then, for a fixed initial droplet temperature of 500°C, measurements were taken during which the pool temperature was increased by 10°C increments until fragmentation no longer occurred. Since no fragmentation was observed for 500°C droplets at a pool temperature of 40°C, no further data were taken for higher pool temperatures. The laboratory data recorded during this set of measurements is given in Table 7.

TABLE 7

LABORATORY DATA FOR DROPPING TIN INTO $^{+}$DISTILLED WATER
(POOL TEMPERATURE VARIED)

(May 16, 1974)

	Temp.		Mass	Geometry			Signal Recorder		Oscilloscope Photos	
Drop No.	Initial Droplet Temp.	Pool Temp.	Load Mass	1 WD	1 DH	1 TD	Recorder Sensitivity	Recorder Delay Time	Time Base	Vertical Sensitivity
#	°C	°C	gm	in	in	in	mv/cm	m/sec	msec/cm	mv/cm
22	700	23	4.617	$21\frac{1}{2}$	$2\frac{3}{16}$	$2\frac{7}{8}$	4	80	20	10
23	700	23	4.619	"	"	"	4	70	20	10
24	700	23	4.627	"	"	"	10	65	20	25
25	700	23	4.609	"	"	"	10	75	20	25
26	700	23	4.623	"	"	"	10	65	20	25
27	700	23	4.621	"	"	"	20	65	20	25
28	500	23	4.608	"	"	"	4	35	10	5
29	500	23	4.621	"	"	"	4	35	10	5
30	500	30.5	4.590	"	"	"	4	35	10	5
31	500	30.5	4.617	"	"	"	4	35	10	5
32	500	30.5	4.629	"	"	"	4	35	10	5
33	500	30.7	4.609	"	"	"	4	35	10	5
34	500	40.3	4.619	"	"	"	4	35	10	5
35	500	40.5	4.628	"	"	"	4	35	10	2.5
36	600	40.0	4.619	"	"	"	4	45	10	2.5
37	600	39.5	4.617	"	"	"	4	35	10	1.0
38	600	39.5	4.625	"	"	"	4	35	10	2.5

TABLE 7 CONTINUED

Drop No.	Results: Good Tape ?	Good Photo ?	2 Visual	3 Audio	Comments
22	√	√	TF	LP	
23	-	√	TF	LP	Tried to capture
24	-	√	TF	LP	Big Bang on tape
25	-	√	TF	LP	
26	-	√	TF	LP	
27	√	√	TF	LP	
28	√	√	TF	LP	
29	√	√	TF	LP	
30	√	√	TF	LP	
31	√	√	TF	SP	Neglected to stir pool
32	√	√	SSF	HNP	Neglected to stir pool
33	√	√	TF	LP	
34	√	√	S-H	HNP	
35	√	√	S-H	HNP	
36	√	√	S-H	HNP	
37	√	√	TF	LP	
38	√	√	S-H	HNP	

[1]See Figure 12 [2]See Table 3 [3]See Table 2

*New Signal Recorder +Same distilled water as on May 14. Still appeared clean

C. Qualitative Results

It will be useful to consider the qualitative results before launching into a quantitative breakdown of the data. Not only is some interesting information obtained in this fashion, but this approach is best used to introduce some concepts and terms that will be used extensively in the subsequent analysis.

The high speed motion pictures showed that when the tin droplets first enter the water pool they begin to flatten at the leading surface and sometimes continue to undergo changes in geometry as they continue to fall through the pool. Due to the fact that a shadow photography technique was employed, the vapor film at the leading surface that was thought to be present could not be distinguished, but vapor along the sides and trailing edge of the droplet could be clearly seen initially. The vapor film was thicker at the tail, and as the entry progressed some vapor bubbles were sometimes observed to detach and migrate to the surface. The lower temperature droplets (300°C and 400°C) appeared to fragment before completely submerging. At the higher initial droplet temperatures, the droplets progressed increasingly deeper into the water before fragmenting. The fragmentation event appeared first as a small explosion at one edge of the droplet, followed by a series of larger magnitude events, until

it appeared that the entire droplet had fragmented. The fragmentation debris appeared initially as a spherical cloud of fine particles (and possibly some vapor) that was observed to undergo several pulsations before drifting appreciably from the fragmentation site. The fragmentation depth as observed in the films was used later to determine the average fall velocity of the droplets through the coolant. No films were taken in this experiment above the coolant cutoff temperature.

Consideration of the appearance of the fragmentation residue as given in Table 6 reveals a clear effect of initial droplet temperature. This is shown in Fig. 13 where it is seen that the well reported pattern of more extensive fragmentation with increasing droplet temperature is borne out. No distinction is made in the table between the nature of the 500°C, 600°C and 700°C fragments, although visual inspection shows the highest temperature debris to be the finest. It is of considerable interest to note the transition that occurs between 300°C and 400°C. The appearance of the 400°C fragments strongly suggests that these were hollow spheroids that were blown open, and further suggests that the same phenomenon producing the 300°C spheroids was acting, only more energetically. Quantitative surface area analysis of the fragments will be performed at a later date.

FIGURE 13

FRAGMENT APPEARANCE AS A FUNCTION OF INITIAL DROPLET TEMPERATURE

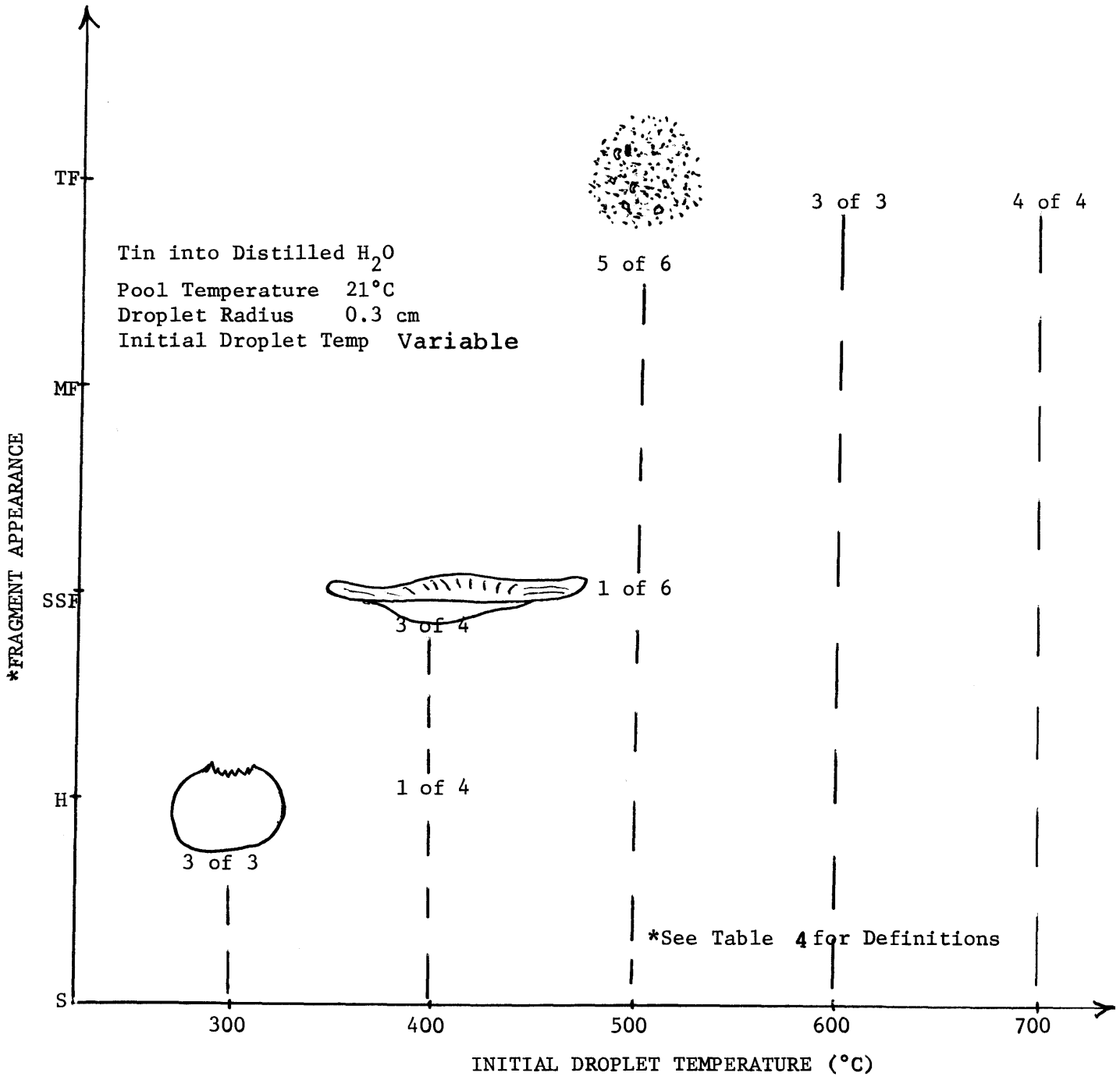

No good explanation can be given for the deviation of the single 400°C and 500°C fragments from the pattern so well established by the other runs.

The effect of increasing the pool temperature on the appearance of the fragments resulting from the 500°C droplets is shown in Figure 14. For pool temperatures of 21°C and 30°C the fragments had virtually the same totally fragmented appearance, but at the pool temperature of 40°C where no extensive fragmentation occurred the residue was solid with several small cavities at the surface. Thus it appears that to produce these cavities a localized phenomenon was acting, even above the coolant cutoff temperature.

A second qualitative trend can be obtained from Table 6 by inspection of the sound characterizing the interactions at the various temperatures. This audio characterization is too subjective to warrant any lengthy consideration here, but it is nevertheless of interest to note that the pop so characteristically heard gets louder as the initial droplet temperature is increased. The quantitative analysis of the pressure recordings given in the following section will lend some more objective backing to this conslusion.

The wealth of the useful data obtained in the present experiment lies in the pressure recordings.

FIGURE 14

FRAGMENT APPEARANCE AS A FUNCTION OF POOL TEMPERATURE

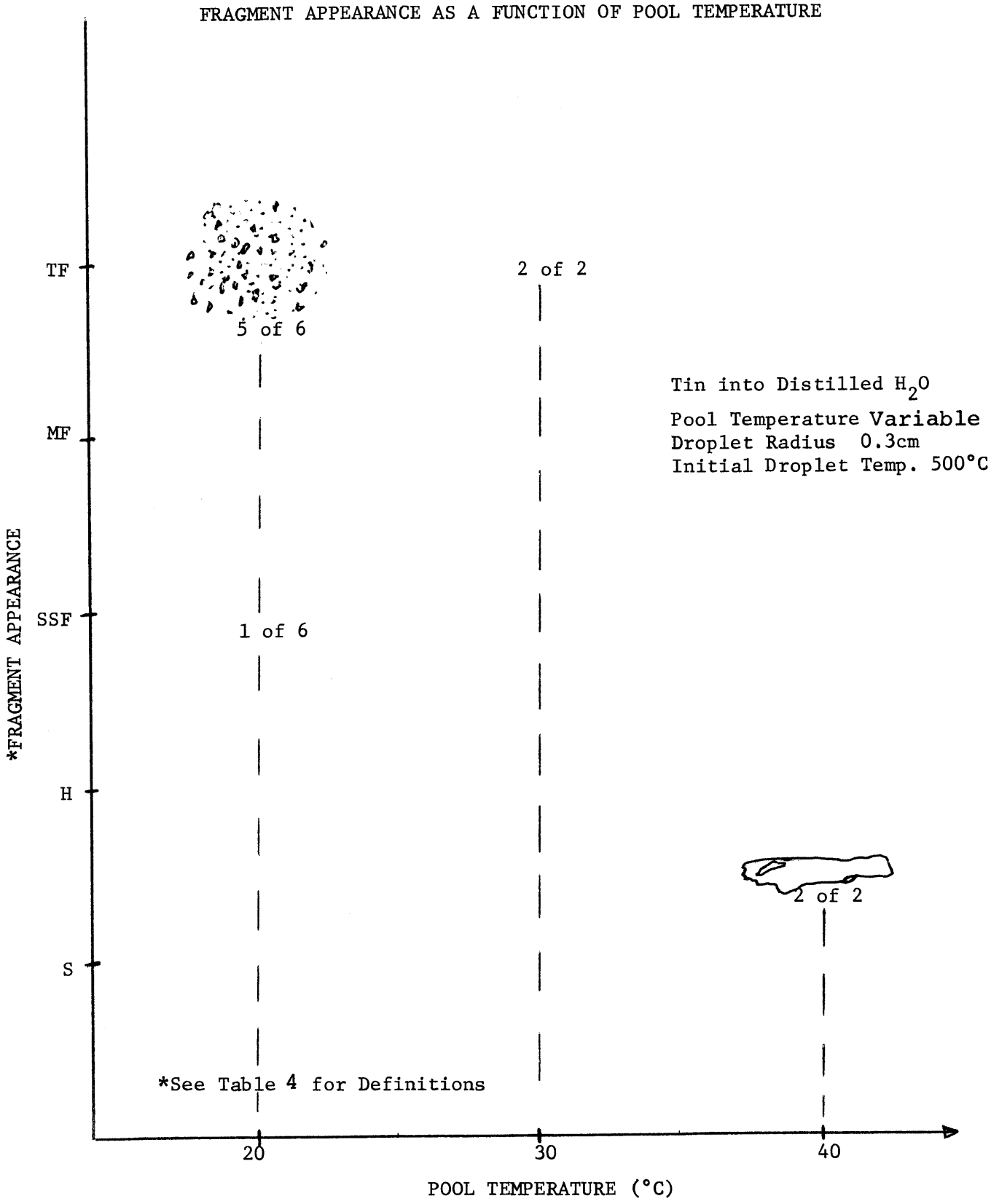

Inspection of the pressure trace photographs allows a qualitative characterization of the interactions at most of the varying initial conditions with little uncertainty. This is done graphically in Figure 15, where for a fixed droplet radius and pool temperature, the qualitative pressure behavior is sketched as a function of time for initial droplet temperatures from 300°C to 700°C.

The pressure trace sketches are used to define some terms that will be extensively used throughout the remainder of this report:

High Frequency (HF) Cycle: A period of high frequency oscillation (greater than about 10 kHz), for which a frequency can usually be determined, that is bounded by droplet entry and a "Quiescent Period".

Quiescent Period: A period of time during which no clear pressure wave of significant magnitude (relative to either the preceding or succeeding portion of the recording) is evident;

Pre-Bang High Frequency (HF) Cycle: A high frequency cycle, during which the Big Bang occurs;

Big Bang: A large magnitude wave of low frequency (less than about 2 kHz) characterizes the so-called 'Big Bang'. This portion of the wave is

FIGURE 15

QUALITATIVE PRESSURE BEHAVIOR
AS A FUNCTION OF
INITIAL DROPLET TEMPERATURE

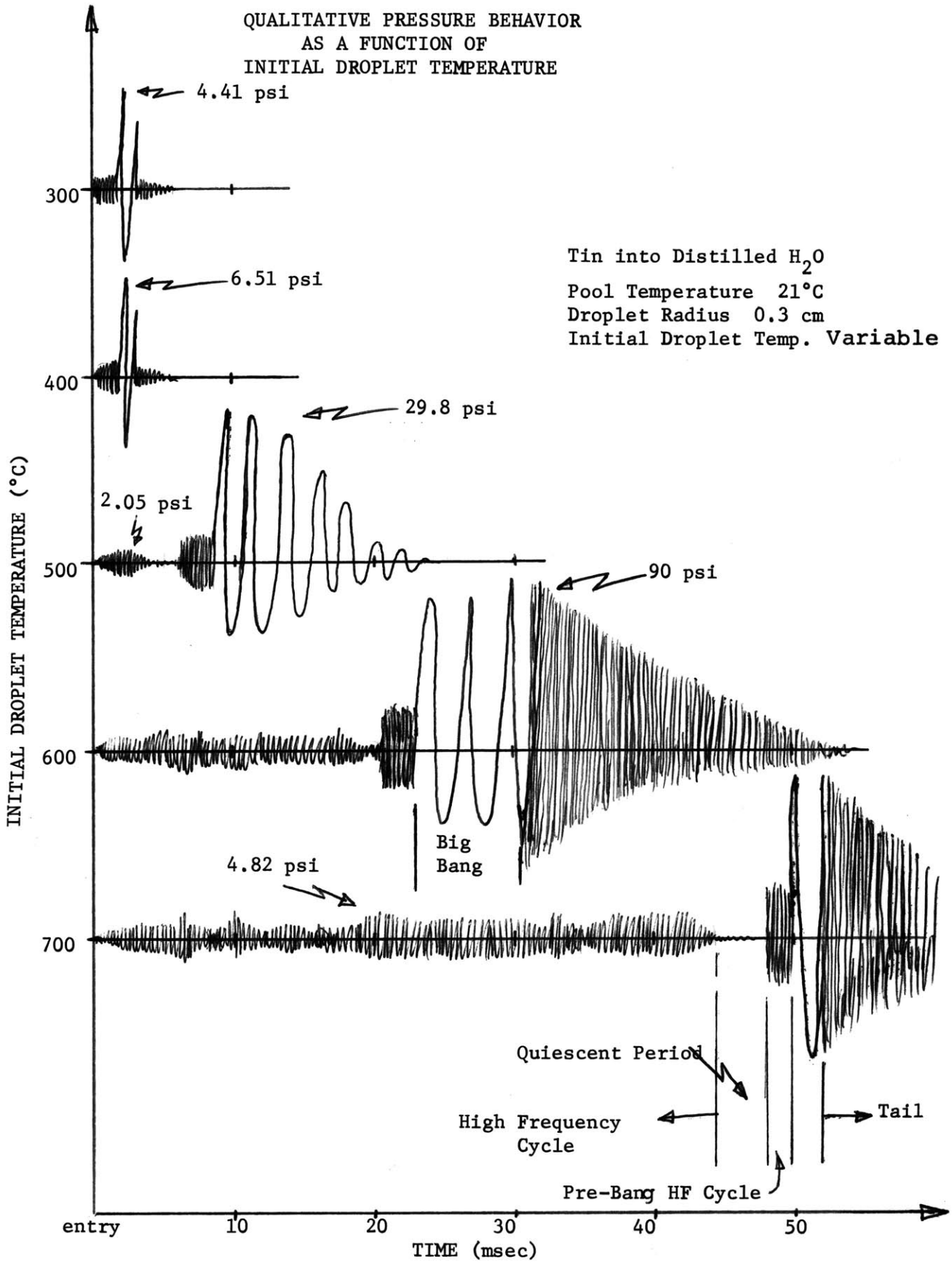

believed to represent the pop that is usually heard to accompany fragmentation, and, when present, is invariably the portion of the wave at which the peak pressure occurs;

Tail: Subsequent to the Big Bang, the pressure decays with time much like a decaying exponential, eventually going to zero as the fragments reach thermal equilibrium with the pool. This tail can either be composed of a high frequency wave as at 600°C and 700°C , or it can be a decaying continuation of the low frequency wave so characteristic of the Big Bang. The latter was usually seen to be the case for initial droplet temperature of 500°C.

Another useful concept is that of the "Dwell Time", which is a measure of the total time that the droplet is submerged in the coolant prior to fragmentation. It is defined here to be quite similar to the dwell time used by Buchanan and Dullforce (8):

Dwell Time: The time interval between droplet entry and the onset of fragmentation, which is taken as the beginning of the Big Bang.

Applying this terminology to the recorded pressure waves leads to some interesting insight into the pressure behavior of the interactions. At the lowest droplet temperatures of 300°C and 400°C, the interaction is char-

acterized by a short duration High Frequency Cycle during which the Big Bang occurs. A cycle or two of Big Bang oscillation is followed by a lower magnitude, higher frequency Tail which rapidly diminishes to an unobservably small magnitude.

At 500°C, an entirely new feature is observed as a High Frequency Cycle beginning the interaction first grows in magnitude, and then diminishes into a short lived period where no pressure wave of significant magnitude is observed. This Quiescent Period is followed by the characteristically abrupt onset of the Pre-Bang HF Cycle which is typically of greater pressure magnitude than the initial HF Cycle. The Big Bang grows out of this Pre-Bang HF Cycle, abruptly lowering the frequency and increasing the pressure to produce a larger magnitude, slower period waveform that was always observed to be present whenever an audible pop was heard during the interaction. The fragmentation event is believed to be associated with the Big Bang portion of the pressure wave. In no case did the Big Bang occur during a Quiescent Period.

The Big Bang is again followed by a decaying Tail for the 500°C droplets. The 600°C and 700°C droplets follow the same general pattern as the 500°C droplets, but differ in that they interact longer and result in greater pressures. It may be significant that the nature of the Tail differed so markedly between the 500°C and the higher temperature

cases. The 500°C Tail exhibited the same general low frequency behavior characteristic of the Big Bang at this same temperature, whereas the Tails of the higher temperature droplets were clearly of a much higher frequency. This may be due either to some type of resonance behavior, or possibly to the fact that the debris cast out by the Big Bang at the higher initial droplet temperatures is itself of high enough temperature to cause new high frequency behavior of significant magnitude.

The qualitative pressure behavior variation with pool temperature is shown in Figure 15 for a constant droplet temperature of 500°C. For coolant temperatures below the coolant cutoff temperature the qualitative pressure behavior is as previously discussed. At a pool temperature of 40°C, however, which is above the cutoff temperature, the pressure behavior is markedly different. The pressure oscillation appears as a long period of low magnitude high frequency oscillation, interrupted at times by the "Little Bangs". These are thought to be the pressure pulses accompanying the production of the small cavities observed in the otherwise solid fragments.

1. Quantitative Assessment of the Temporal Pressure Behavior

Application of the definitions of pressure wave characteristics given in the previous section (see Figure 14) to the photographed pressure recordings yielded the values

FIGURE 15A

QUALITATIVE PRESSURE BEHAVIOR
AS A FUNCTION OF
POOL TEMPERATURE

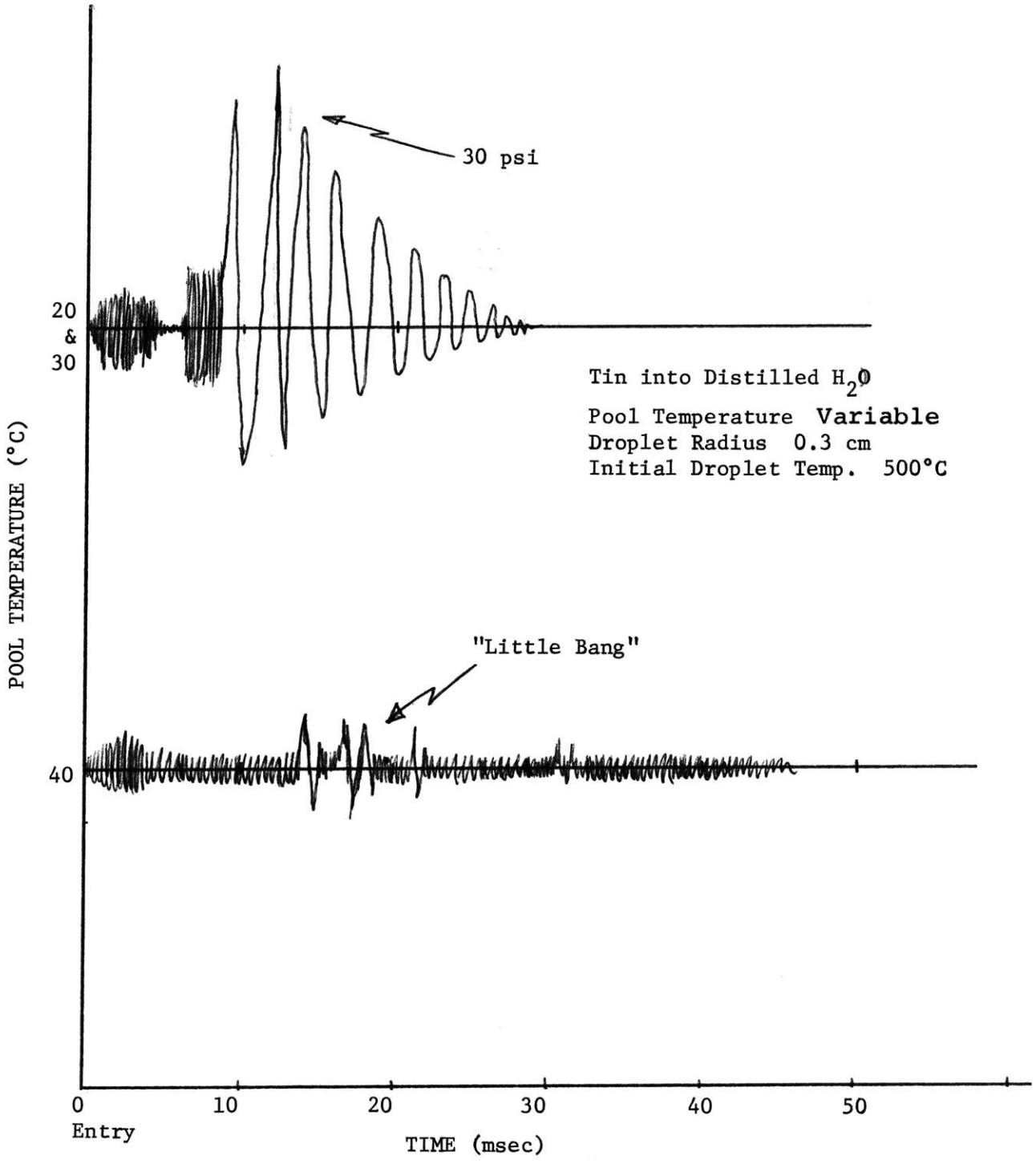

given in Table 8. Uncertainties in the interpretation of the oscilloscope photographs preclude the use of the values given for fine comparisons, but the results are nevertheless useful for the determination of gross trends. Those waveforms not exhibiting a particular feature resulted in an NA (for "Not Applicable") being recorded in the corresponding column, whereas if the required information could not be determined, or if the waveform did not exhibit any of the defined features, a dash (-) was recorded. Averages were then taken where appropriate to give an indication of the expected behavior for each particular set of initial conditions. When these averaged results are used to draw the averaged qualitative behavior Figure 14 is produced, where the time behavior is drawn to scale but the pressure scale is varied.

A useful indicator of the time required for fragmentation to occur is the dwell time. Figure 16 presents the average dwell time plotted as a function of initial droplet temperature (for constant pool temperature and droplet radius). There is an insignificant difference between the dwell times of the 300°C and 400°C droplets, with a clear trend to increasing dwell time with increasing droplet temperature starting at a droplet temperature of 400°C. These data are in close agreement with the results obtained by Buchanan and Dullforce (8).

TABLE 8

QUANTITATIVE BREAKDOWN OF TEMPORAL BEHAVIOR OF THE COOLANT PRESSURE WAVES

Case No. (#)	Initial Droplet Temp. (°C)	Pool Temp. (°C)	1 HFC Duration (msec)	$\bar{1}$ Avge. HFC Duration (msec)	2 QP Duration (msec)	$\bar{2}$ Avge. QP Duration (msec)	3 Pre-Bang HFC Duration (msec)	$\bar{3}$ Avge. Pre-Bang HFC Duration (msec)	4 Big Bang Duration (msec)	$\bar{4}$ Avge. Big Bang Duration (msec)	5 HF Tail Duration (msec)	$\bar{5}$ Avge HF Tail Duration (msec)	6 Dwell Time (msec)	$\bar{6}$ Avge. Dwell Time (msec)
1	300	21	NA	NA	NA	NA	0.9	1.35	0.4		2.5		0.9	
2	300	21	NA	NA	NA	NA	1.8	(2)	2.0	1.2	--	2.5	1.8	1.35
3	300	21	NA	NA	NA	NA	--		--	(2)	--	(1)	--	(2)
4	400	21	NA	NA	NA	NA	1.0	1.4	0.6		1.0		1.0	
5	400	21	NA	NA	NA	NA	0.8	(3)	0.7	0.67	--	2.5	0.8	1.4
6	400	21	NA	NA	NA	NA	2.4		0.7	(3)	4.0	(2)	2.4	(3)
20	400	21	NA	NA	NA	NA	--		--		--		00	
7	500	21	--		--		--		--		--		00	
8	500	21	2		4		2		14	16	NA	20(1)	8	
9	500	21	4	3.6	2	2,4	2	2	6	(3)	20	NA	8	8
10	500	21	4	(5)	2	(5)	NA	(4)	NA	6(1)	NA	(4)	NA	(4)
11	500	21	2		4		2	NA	10	NA	NA		8	NA
21	500	21	6		0		2	(1)	24	(1)	NA		8	(1)
12	600	21	NA	NA	NA	NA	20	19	8		24	23.0	20	
13	600	21	NA	NA	NA	NA	18	(2)	8	8(3)	20	(3)	18	23
19	600	21	28	28(1)	0	0	4	4(1)	8		24		32	(3)
14	700	21	--		--		--		--		--		--	
15	700	21	--	44	--	4	--	4	--	4	--	26	--	52
16	700	21	--	(1)	--	(1)	--	(1)	--	(1)	--	(1)	--	(1)
18	700	21	44		4		4		4		26		52	

TABLE 8 CONTINUED

Case No. (#)	Initial Droplet Temp. (°C)	Pool Temp. (°C)	HFC Duration (msec)	Avge. HFC Duration (msec)	QP Duration (msec)	Avge. QP Duration (msec)	Pre-Bank HFC Duration (msec)	Avge. Pre-Bang HFC Duration (msec)	Big Bang Duration (msec)	Avge. Big-Bang Duration (msec)	HF Tail Duration (msec)	Avge. HF Tail Duration (msec)	Dwell Time (msec)	Avge. Dwell Time (msec)
28	500	23	6	6	2	1.5	2	2.5	6	6(1)	10	10(1)	10	10
29	500	23	6	(2)	1	(2)	3	(2)	20	20(1)	NA	NA(1)	10	(2)
22	700	23	34		2		2		4		26		38	
23	700	23	32	34	2	4.7	6	3.3	4		32		40	
24	700	23	36	(3)	10	(3)	2	(3)	4	4.7	28	27.7	48	36.7
25	700	23	NA	NA	NA	NA	32	31.3	8	(6)	24	(6)	32	(6)
26	700	23	NA	(3)	NA	(3)	32	(3)	4		28		32	
27	700	23	NA		NA		30		4		28		30	
30	500	30.5	3		5		1		12		NA		9	
31	500	30.5	--	2.5	--	5.5	--	1.5	--	17	--	NA	--	9.5
32	500	30.5	--	(2)	--	(2)	--	(2)	--	(2)	--		--	(2)
33	500	30.7	2		6		2		22		NA		10	
34	500	40.3	--		--		--		--		--		--	
35	500	40.5	--		--		--		--		--		--	
36	600	40.0	--		--		--		--		--		--	
37	600	39.5	--		--		--		--		--		--	
38	600	39.5	--		--		--		--		--		--	

NA = not applicable -- = datum not available

TAB 5/26/74

FIGURE 16

DWELL TIME VS. INITIAL DROPLET TEMPERATURE

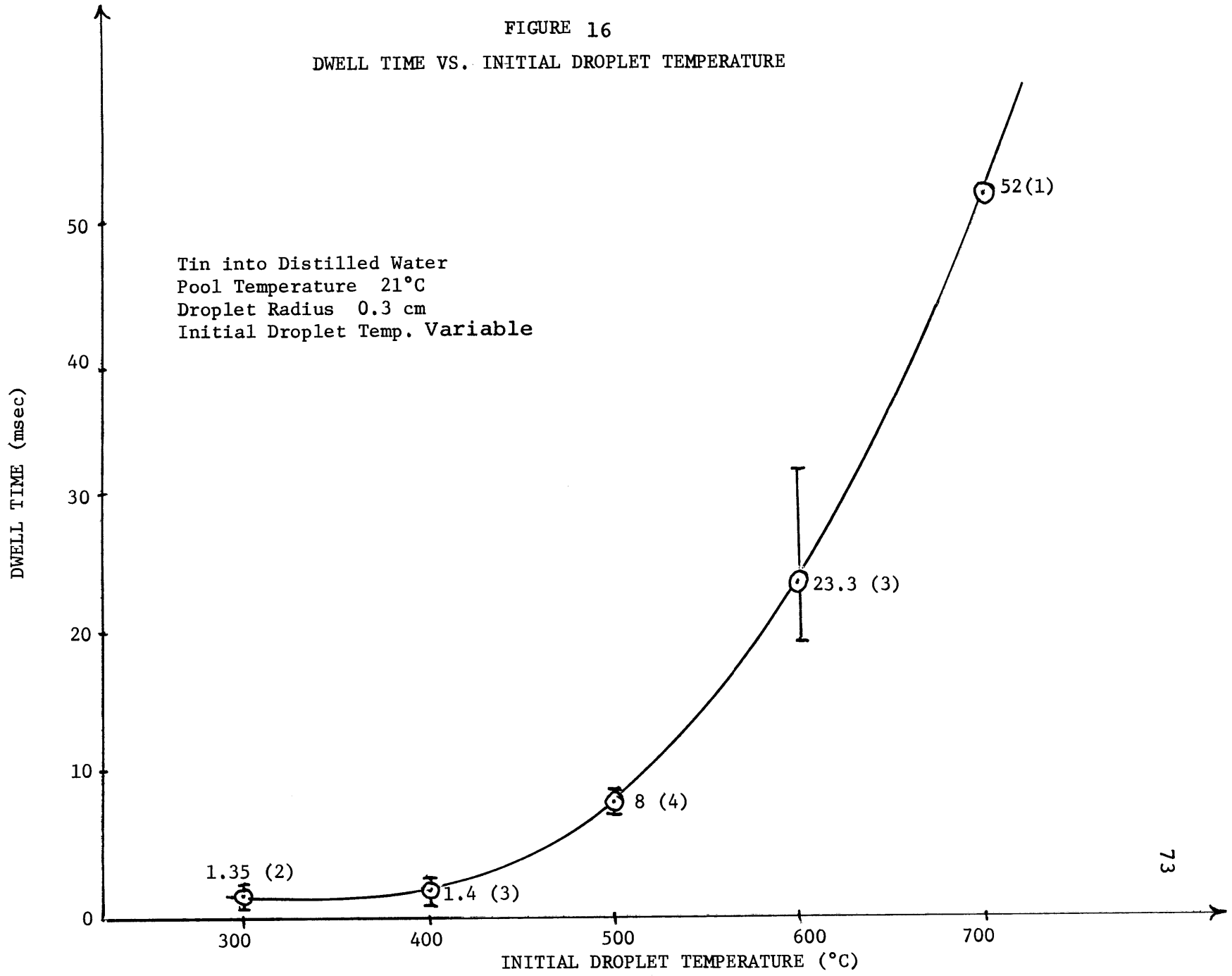

Comparison of the average dwell times for the 500°C droplets at the pool temperatures of 21°C, 23°C and 30°C indicates no significant change in dwell time with pool temperature over this range. This is shown in Figure 17. No dwell times could be determined for the 500°C droplets at a pool temperature of 40°C since no Big Bang (Fragmentation) was observed to occur.

2. Quantitative Assessment of Pressure Magnitude Behavior

The only definitive source of data for determining the quantitative pressure behavior was the recorded tapes, each containing a maximum of only 20 msec of information. Those cases for which quantitative data could be obtained are included in Table 9, which gives the pertinent initial conditions as well as the observed pressure magnitudes. The maximum Big Bang pressure is entered in Column 1 as measured at the transducer and as determined from the tape recording. Column 2 contains the peak pressure observed during the High Frequency Cycle for a given run. Some manipulation of these figures is required before the pressure magnitude at the surface of the droplet can be obtained, however, since the measured pressures were obtained at varying distances from the droplets.

By making use of both the high speed motion pictures taken for cases 18 through 21 and the observed dwell times, an average velocity of 30.8 inches/second was determined

FIGURE 17

DWELL TIME VS. POOL TEMPERATURE

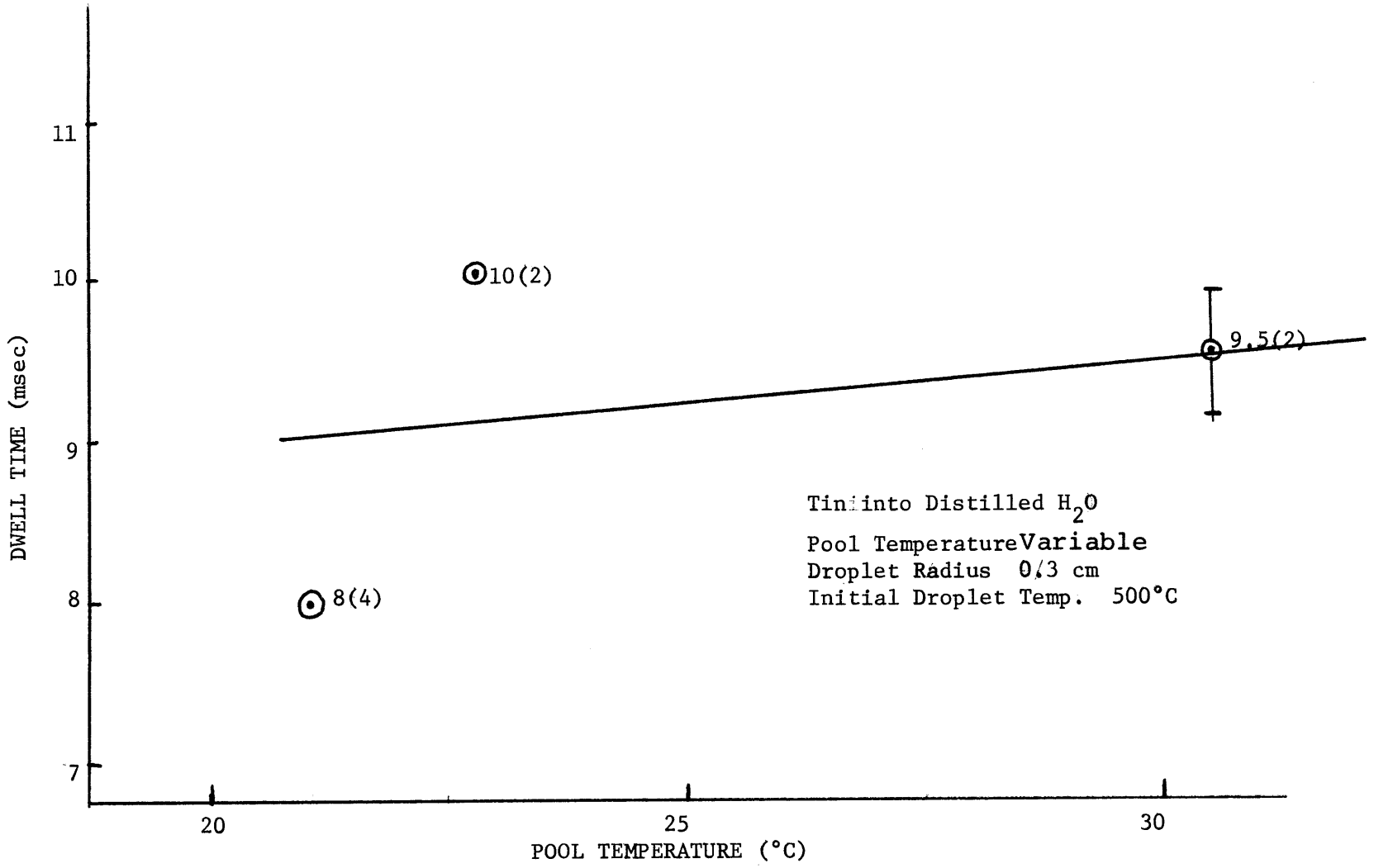

TABLE 9

QUANTITATIVE PRESSURE MAGNITUDE RESULTS

Case No. (#)	Transducer Depth (in.)	Initial Droplet Temp. (°C)	Pool Temp. (°C)	Recorded Peak BB Pressure (psi)	Recorded Peak HF Pressure (psi)	Peak BB Pressure at Droplet Surface (psi)	Peak HF Pressure at Droplet Surface (psi)	Average Peak BB Pressure at Surface (psi)	Average Peak HF Pressure at Surface (psi)
1	2.19	300	21	0.34	0.017	6.3	0.315		
2	2.19	300	21	0.136	0.034	2.52	0.620	4.41	0.69
3	2.19	300	21	--	0.061	--	1.13	(2)	(3)
4	2.19	400	21	0.34	0.068	6.3	1.26		
5	2.19	400	21	0.34	0.034	6.3	0.63	6.51	1.05
6	2.19	400	21	0.374	0.068	6.93	1.26	(3)	(3)
9	2.19	500	21	1.96	--	32.6	--		
10	2.19	500	21	--	0.085	--	1.41	29.8	2.05
11	2.19	500	21	1.62	0.162	27.0	2.69	(2)	(2)
12	4.25	600	21	1.96	--	59	--	90(2)	--
13	4.25	600	21	4.25	--	128	--		--
15	4.25	700	21	--	0.19	--	4.82	--	4.82(1)
27	2.88	700	23	11.9	--	164	--	164(1)	--
28	2.88	500	23	1.02	0.06	22.9	1.35	34.4	1.6
29	2.88	500	23	1.53	0.08	34.4	1.8	(1)	(2)
30	2.88	500	30.5	1.02	0.068	22.9	1.53	29.7	1.45
33	2.88	500	30.7	1.62	0.061	36.4	1.37	(2)	(2)
34	2.88	500	40.3	--	0.05	--	1.12	--	1.12(1)
36	2.88	600	40.0	--	0.255	--	4.69	--	5.79
37	2.88	600	39.5	--	0.374	--	6.88	--	(2)

for the droplets falling through the coolant. Assuming the average velocity to be the same at all droplet and coolant temperatures, and further assuming that the acoustic source was in all cases a sphere with a radius of 0.3 cm, a correction was made to the recorded pressure to give the actual pressure at the surface of the droplet. The calculations were performed by making use of the relation obtained by utilizing equation 8 and expressing r in terms of geometric and measured parameters:

$$p(a) = \frac{(TD - \bar{v}\ \Delta t_{swell})}{a}\ p(r) \quad , \tag{9}$$

where TD is the transducer depth, $\bar{v}$ is the average droplet velocity, Δt_d is the dwell time, a is the sphere radius, and p(r) is the recorded pressure at the transducer. The resulting droplet surface pressures are given in columns 3 and 4 of Table 9, with the averages for a given set of initial conditions given in columns 5 and 6.

Figure 18 is a plot of the observed effect of initial droplet temperature on the peak high frequency pressure at the droplet surface. The results given are for a constant pool temperature of 21°C and a fixed droplet radius of 0.3 cm. This figure shows that there is a clear trend of increasing pressure with increasing initial droplet temperature.

FIGURE 18

THE OBSERVED EFFECT OF INITIAL DROPLET TEMPERATURE
ON PEAK HIGH FREQUENCY PRESSURE

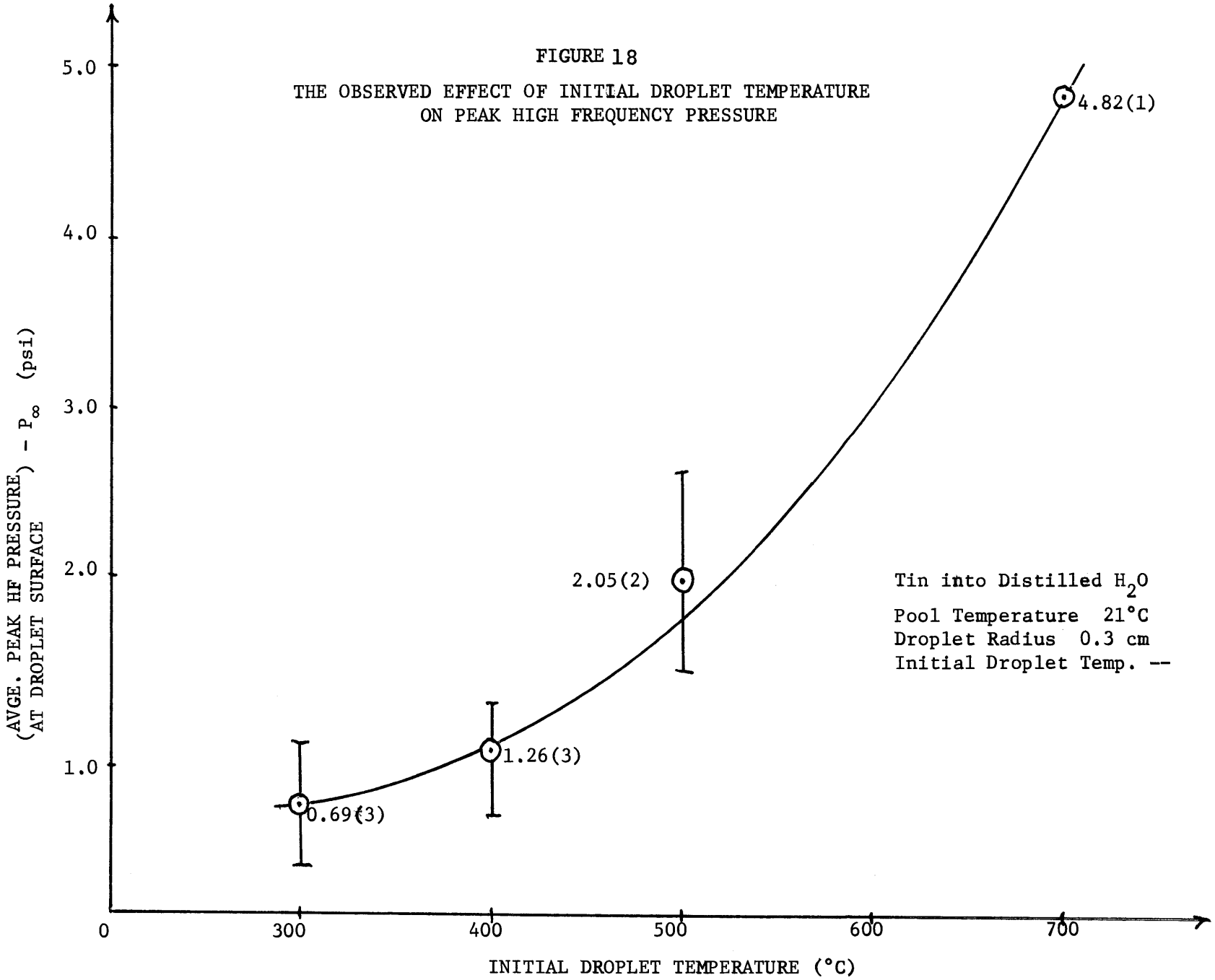

The observed effect of the water pool temperature on the peak high frequency pressure is shown in Figure 19. Here the droplet radius and initial temperature are held constant at 0.3 cm and 500°C, respectively, while the pool temperature was varied. There appears to be a trend of decreasing pressure with decreased water subcooling, although this is by no means a dramatic effect over this particular range of pool temperature. It may be significant that one of the two data points used to calculate the average peak pressure at a pool temperature of 21°C (point #10) was not characteristic of the interaction observed for the other 5 runs made at this same pool temperature (see Table 6). Ignoring this point results in a more distinct pressure decrease with increasing pool temperature.

Figures 18 and 19 are particularly significant in that they present the experimental pressure magnitude data against which the calculations of the acoustic cavitation theory will be measured. The comparison will be made in the following section.

A plot of the maximum observed pressure as a function of initial droplet temperature is given in Figure 20. The pool temperature is constant at 21°C and the droplet radius is fixed at 0.3 cm. Increasing the initial droplet temperature results in a clear increase in the maximum observed pressure. Although no definitive recordings were obtained

FIGURE 19

THE OBSERVED EFFECT OF POOL TEMPERATURE ON PEAK HIGH FREQUENCY PRESSURE

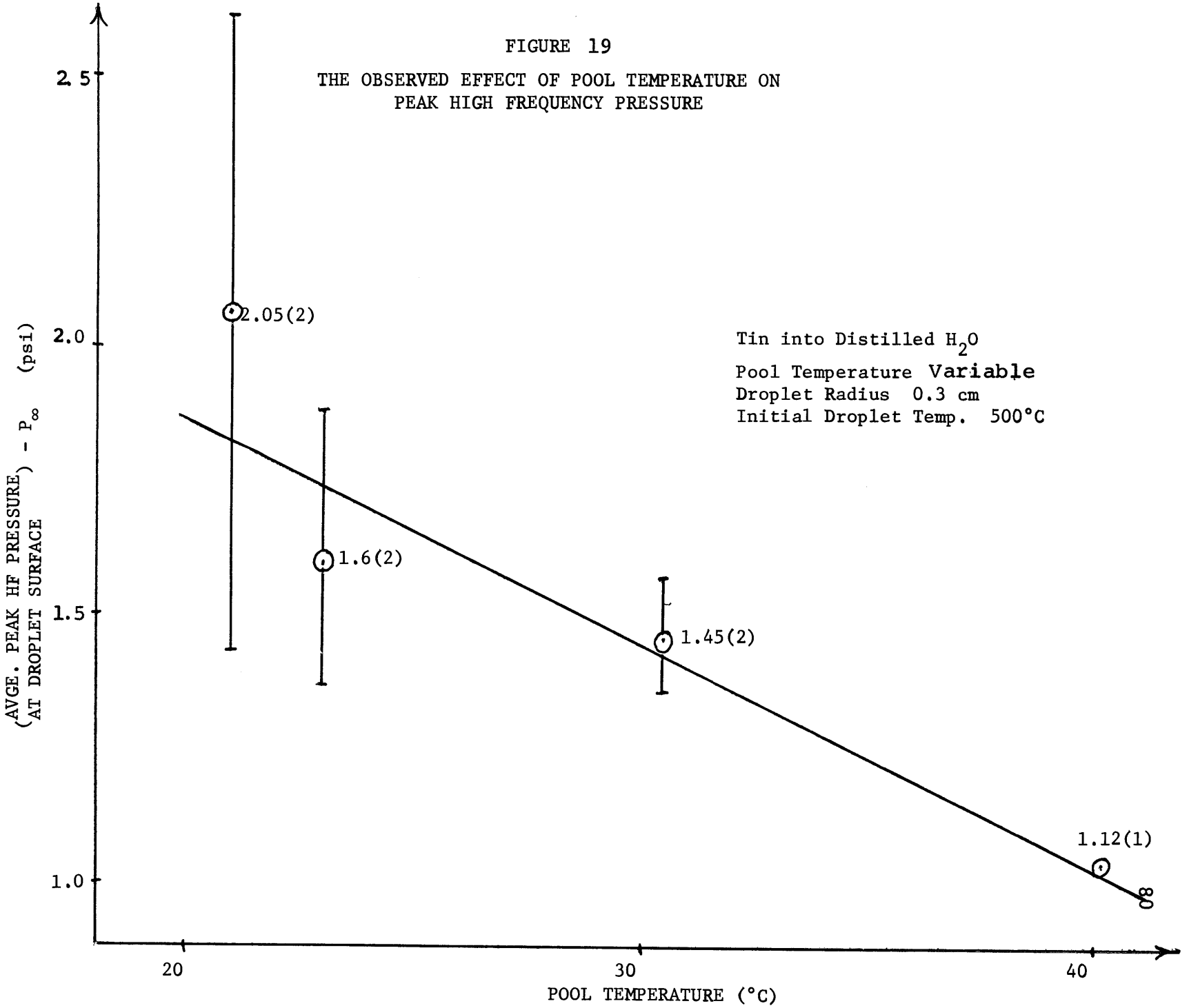

FIGURE 20

THE OBSERVED EFFECT OF INITIAL DROPLET TEMPERATURE ON *MAXIMUM PRESSURE

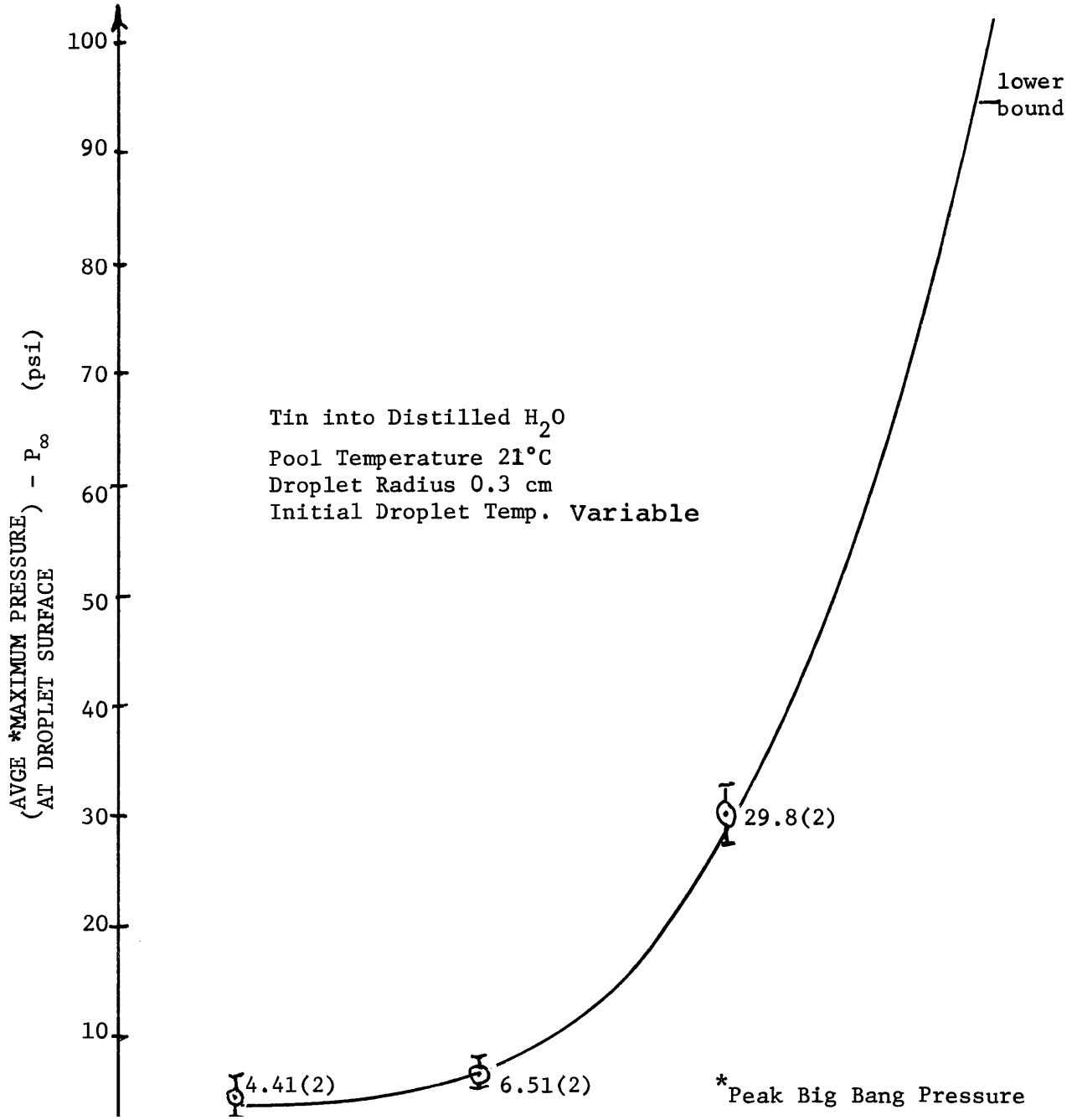

for droplet temperatures of 600°C and 700°C for this particular pool temperature, the two recordings obtained at 600°C indicate that the average peak pressure at this temperature must be at least 94 psi.

Figure 21 demonstrates the observed effect of pool temperature on the maximum pressure for a fixed droplet radius of 0.3 cm and an initial droplet temperature of 500°C. The data plotted span the coolant cutoff temperature above which no fragmentation occurred, and this is the reason for the large decrease observed between pool temperatures of 30°C and 40°C. At coolant temperatures below 30°C fragmentation occurred and the maximum pressure plotted is the peak Big Bang pressure. At 40°C no fragmentation occurred, and the maximum pressure plotted is consequently the peak HF pressure. The coolant cutoff temperature for 500°C tin droplets of 0.3 cm radius is therefore somewhere between 30°C and 40°C. No attempt was made to more precisely determine the exact cutoff temperature.

3. Quantitative Frequency Behavior

The determination of frequencies apparent in the recorded waveforms was performed using both an oscilloscope and the Nelson Ross spectrum analyzer described earlier. The recorded waveforms were first played through the oscilloscope in order to obtain a visual estimate of the high frequencies whenever possible. This was difficult

FIGURE 21

THE OBSERVED EFFECT OF POOL TEMPERATURE ON MAXIMUM PRESSURE

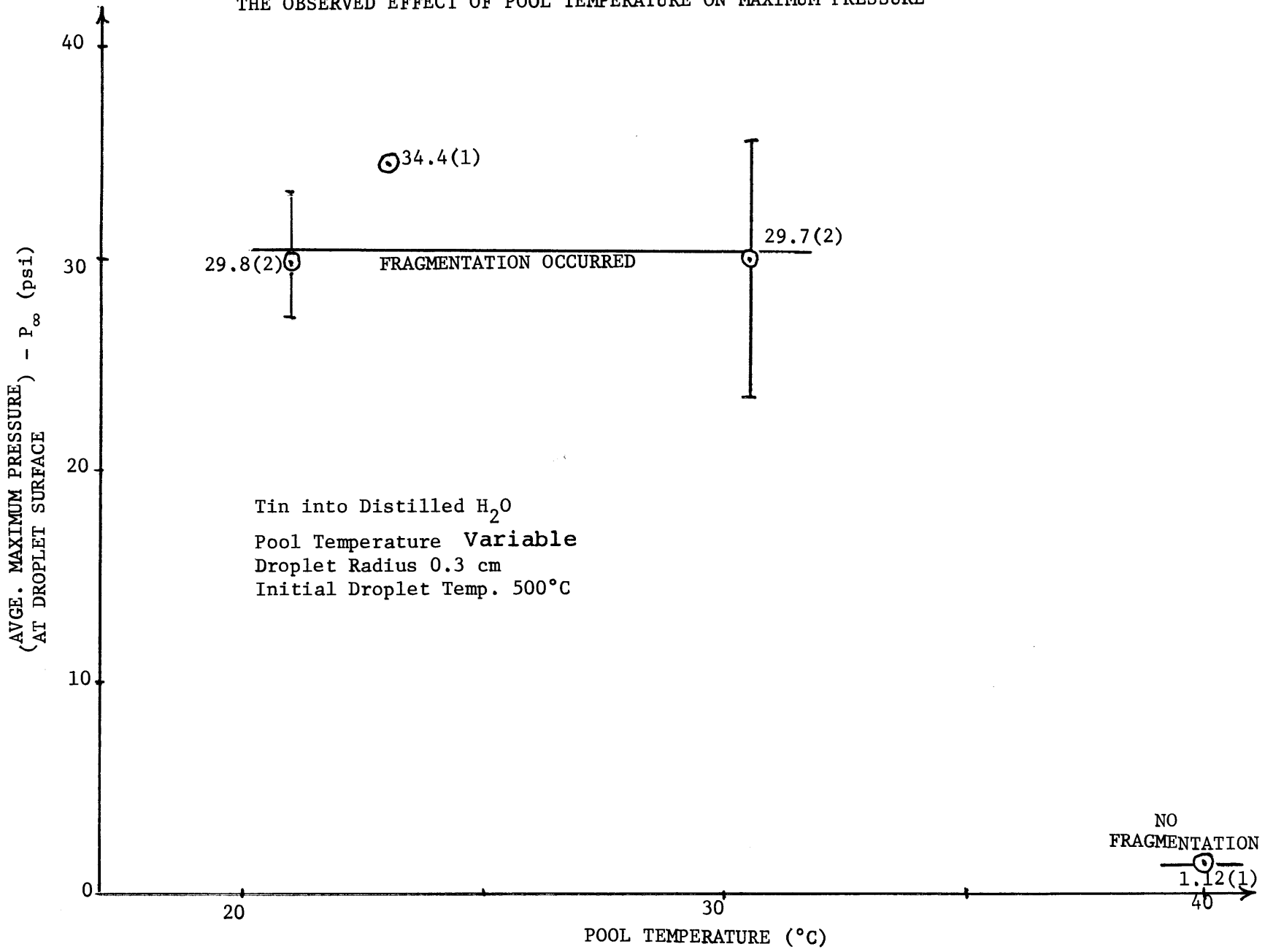

to do in some cases where the waveform frequency did not appear to be clearly defined, due either to the low pressures or to the nature of the waveform itself. The frequency obtained in this fashion was then used as a guide in interpreting the output from the spectrum analyzer, which defines the frequencies for which the input waveform exhibits corresponding components. Averaging of close lying frequency peaks from the spectrum analyzer were then taken to produce the averaged dominant frequencies given in column 4 of Table 10. Column 2 of Table 10 contains the Big Bang frequency obtained from the spectrum analyzer in a similar fashion.

Increasing the initial droplet temperature is seen in Figure 22 to decrease the observed frequency of the Big Bang above initial droplet temperatures of 400°C, whereas no significant effect is observed below 400°C. Figure 22 is drawn for a constant pool temperature of 21°C and a droplet radius of 0.3 cm.

Data for a fixed initial droplet temperature of 500°C and a radius of 0.3 cm is plotted as a function of pool temperature in Figure 23. It should be pointed out that the range of pool temperature reported here is only 10°C, so caution must be exercised in drawing any far reaching conclusions. Nevertheless, there does appear to be a slight trend of decreasing frequency with increasing coolant temperature.

TABLE 10

PRESSURE FREQUENCY DATA

Case No. (#)	Initial Droplet Temp. (°C)	Pool Temp. (°C)	1 *Big Bang Frequency (Hz)	2 Average Big Bang Frequency (Hz)	3 †Dominant High Frequency (kHZ)	4 ≠Average Dominant High. Frequ. (kHZ)	5 Visual HF Determination (kHZ)
1	300	21	1800	1750	15.4	14.2	--
2	300	21	1700	(2)	13.0	(2)	--
4	400	21	1760	1730	--		--
5	400	21	1760	(3)	18.0	17.7	--
6	400	21	1680		17.4	(2)	--
9	500	21	1200	1200	15.0		--
10	500	21	--	(3)	18.1	16.6	16.5
11	500	21	920,1480		16.8	(3)	12.8
12	600	21	720	720	15.9	16.2	15
13	600	21	--	(1)	16.5	(2)	15.3
15	700	21	--	--	12.5	12.5(1)	12.0
28	500	23	800	800	--	17.0	9.8
29	500	23	800	(2)	17.0	(1)	14.7
22	700	23	--		12.0	12.0	--
27	700	23	†620	(1)	00	(1)	--
30	500	30.5	800		00		13.5
31	500	30.5	--	720	12.0	11.0	10.4
32	500	30.5	--	(2)	10.0	(2)	10.4
33	500	30.7	640		--		13.8
34	500	40.3	- -	--	10.6	11.6(1)	11.0
36	600	40.0	--	--	10.0	10.0	10.4
37	600	39.5	--	--	10.0	(2)	10.6

* As determined by spectrum analyzer

† From photograph of tape record. Average over 2 cycles

≠ High Frequency Cycle or Pre-Bang High Frequency Cycle

FIGURE 22

THE OBSERVED EFFECT OF INITIAL DROPLET TEMPERATURE ON BIG BANG FREQUENCY

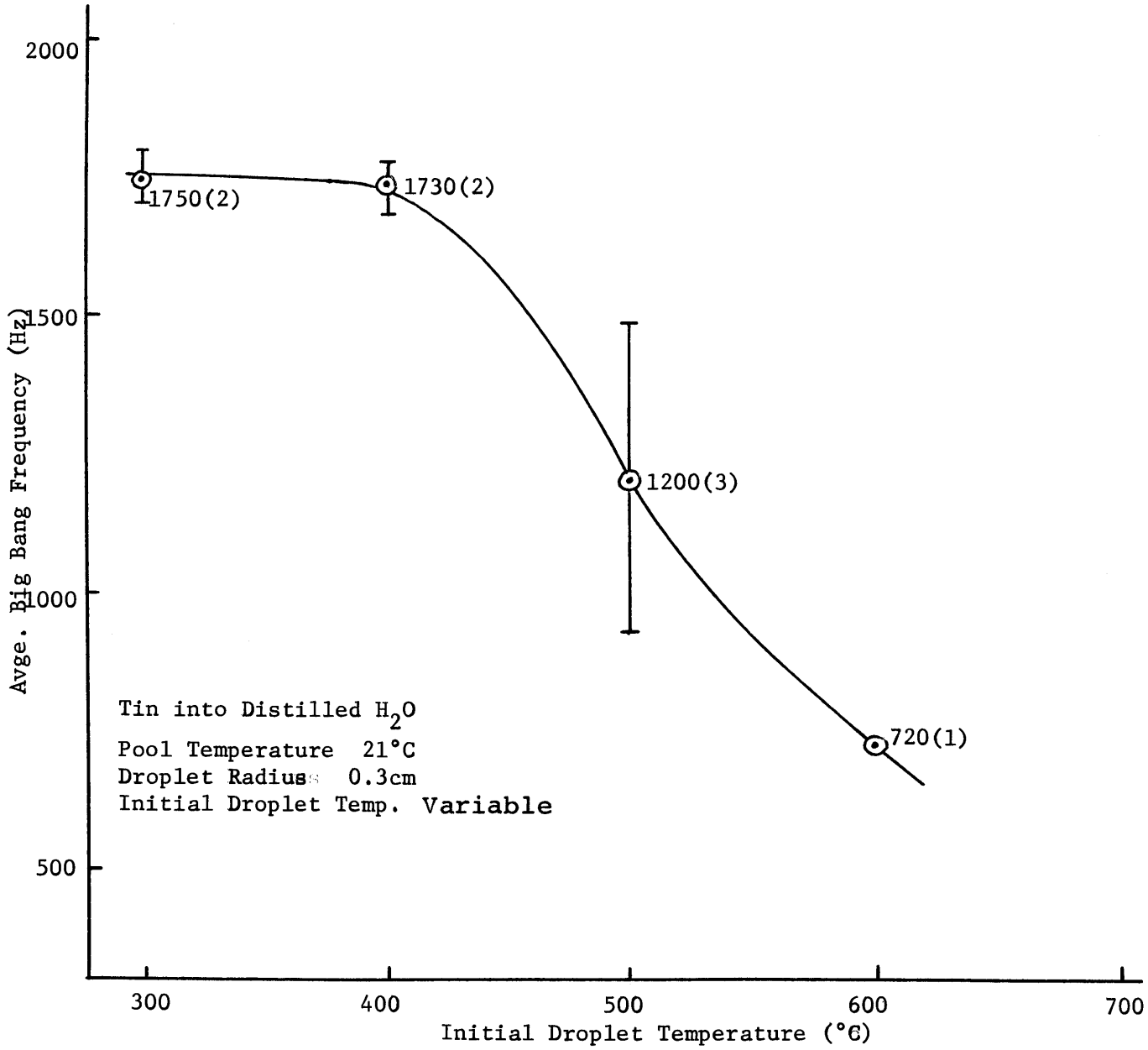

FIGURE 23

THE OBSERVED EFFECT OF POOL TEMPERATURE ON BIG BANG FREQUENCY

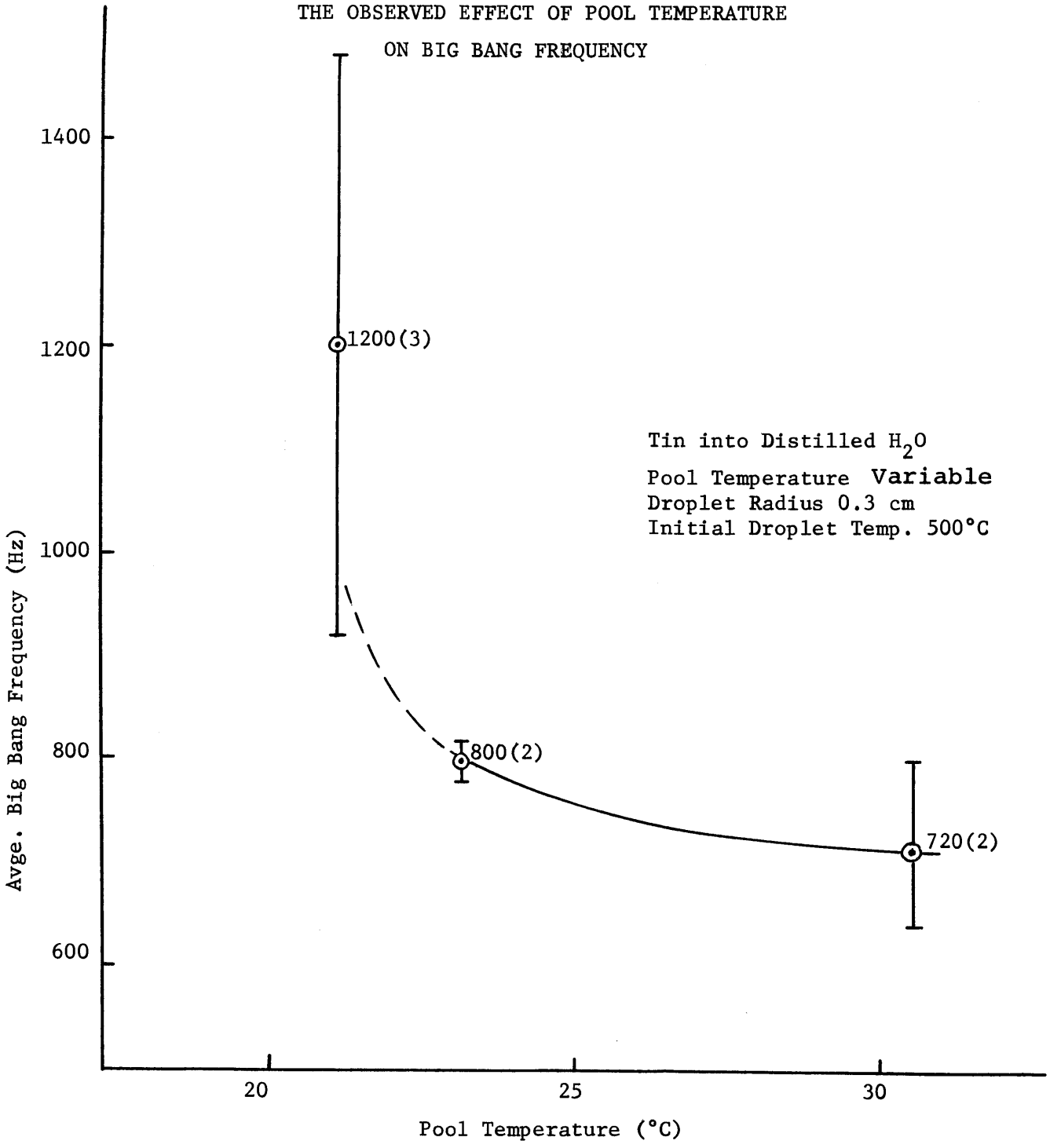

Figure 24 reveals an interesting effect on the frequency of the high frequency portion of the pressure wave due to variation in the initial droplet temperature. As the droplet temperature is increased from 400°C, the frequency clearly decreases. In the range from 300°C to 400°C, however, a frequency increase with increasing droplet temperature is evident. Due to the facts that the magnitude of the high frequency pressure at the 300°C droplet temperatures was so small, and the duration of the high frequency waveform was so short (see Table 8), no great confidence should be placed in these 300°C results. It is significant, however, that the two 300°C cases for which data were obtained corroborate the validity of this point.

Finally, the observed effect of the pool temperature on the frequency is displayed in Figure 25 for both the 500°C and 600°C initial droplet temperatures. The effect at both droplet temperatures appears to be the same, with increasing pool temperature causing a decrease in the observed high frequencies.

4. Possible Sources of Variability and Error

A potentially significant source of error existed in the present experiment which has to do with the temperature of the droplets. It was pointed out earlier that the molten tin droplets were produced by immersing the stainless steel crucible containing a solid tin slug of care-

FIGURE 24

THE OBSERVED EFFECT OF INITIAL DROPLET TEMPERATURE ON *HIGH FREQUENCY

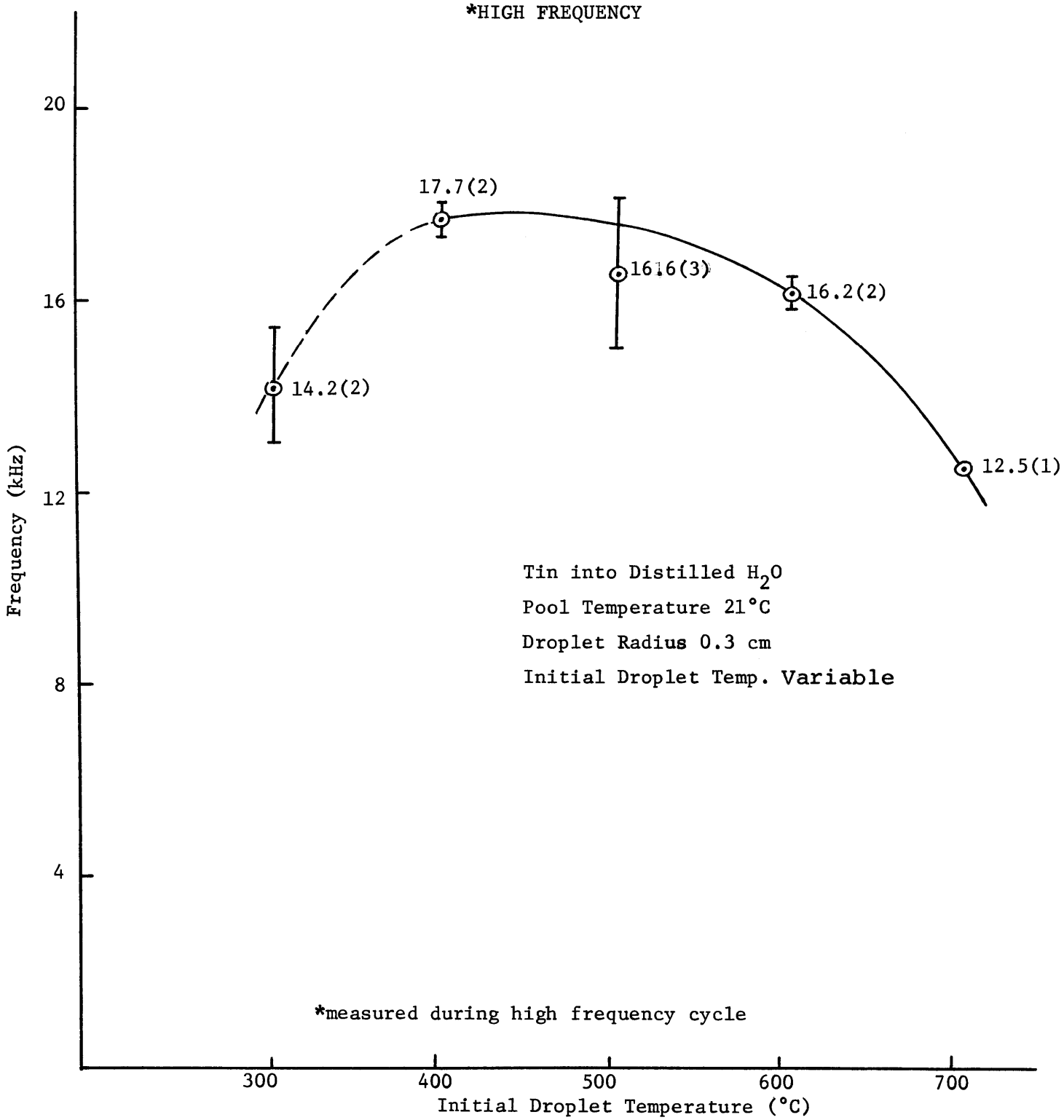

FIGURE 25

THE OBSERVED EFFECT OF POOL TEMPERATURE

ON **HIGH FREQUENCY

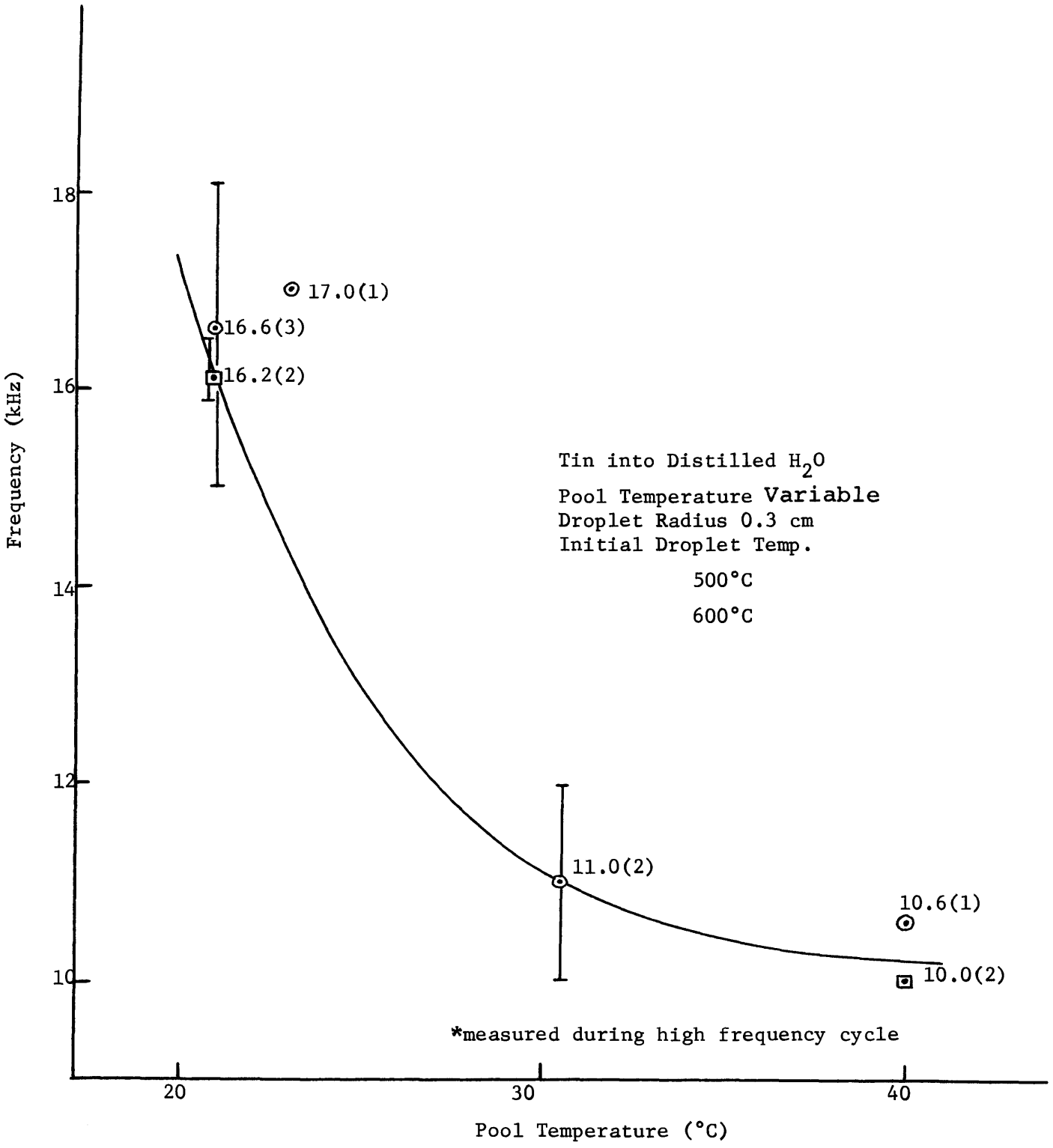

fully controlled mass in the core of a 5 kw electric furnace. This method of heating is conducive to the production of thermal gradients within the tin, and may therefore have resulted in varying initial droplet temperatures, especially for the higher droplet temperatures where the rate of cooling is greater. The variability observed in the results is probably due largely to this effect.

D. Comparison of Results with Predictions of the Acoustic Cavitation Theory

The results obtained in the present experiment can be used as a measure of the accuracy with which the model developed by Kazimi predicts the observed film pressure behavior.

The logical first step is to compare the observed qualitative pressure behavior as depicted in Figure 14 to the calculated film pressure behavior shown in Figure 2. The applicable section of the recorded waveforms is the behavior prior to fragmentation only, since Kazimi's calculations do not extend beyond the point where fragmentation begins. It is immediately apparent that the general qualitative agreement is poor, particularly the early pressure behavior. Where Kazimi's model predicts the peak pressure to occur on the first cycle, the high frequency pressure is observed to build gradually over the first few cycles. Consideration of the facts that it actually takes a spherical droplet about 6 msec to completely submerge after free falling from a height of 2 inches and that Kazimi's model assumes instantaneous submergence, leads one to expect poor agreement in this 'entry regime'.

It is also apparent that at the higher temperatures the recorded high frequency cycles exhibit a period of relatively constant amplitude, whereas the calculations

predict a decreasing amplitude. This difference may be due to the fact that the actual droplets are immersed in a velocity field with an observed vapor tail. If vapor is streaming around the droplet from the leading surface, then this difference may be due to a relatively constant film thickness at the leading edge where the pressure is being measured. Kazimi's calculations predict a dynamically growing film, with the pressure decreasing as the film grows thicker. None of the high speed movies taken to date provided the definition of the vapor film thickness necessary to determine the validity of this explanation.

Finally, Kazimi's calculations do predict that some point should be reached in the pressure history at which no significant pressure wave should be evident. Under the assumption that the Quiescent Periods observed in the higher temperature cases are indeed representative of just such a point, then the theory appears to have been successful in this respect. Kazimi's model does not, however, predict any subsequent interaction.

Insofar as Kazimi's calculations appear to extend only as far as the Quiescent Period, no further significant qualitative comparisons can be made. Numerous quantitative comparisons are possible, however, providing the fundamental assumption is made that the predicted pressure wave corresponds to the observed high frequency oscillation that precedes fragmentation.

Data are now available that give the effect of both the initial droplet temperature and water pool temperature on both the frequency and magnitude of the pressure.

Turning first to the effect of pool temperature, some interesting results are obtained. The predicted effect is for increasing pool temperature to decrease the film pressure frequency as shown in Figure 3. The observed effect of increasing the pool temperature is shown in Figure 25, and again in the upper left hand quadrant of Figure 26, to be similar over the range of coolant temperatures investigated although the data seem to indicate a leveling off at a pool temperature of 40°C. The actual frequency of about 16.6 kHz for the 500°C droplet agrees well with the averaged frequency of 17.5 kHz obtained for the corresponding portion of the predicted case (see Figure 2).

Increasing the pool temperature is further calculated to increase the peak film pressure (see Figure 3). This is clearly contrary to the observed decrease in peak pressure as shown in Figure 19. This is a significant disagreement between the theory and experiment for which no satisfactory explanation can currently be given. These results are given in juxtaposition in the lower left hand quadrant of Figure 26. The quantitative agreement is also poor here, with the predicted peak film pressure for a 500°C droplet of radius 0.3 cm in water at 20°C being about

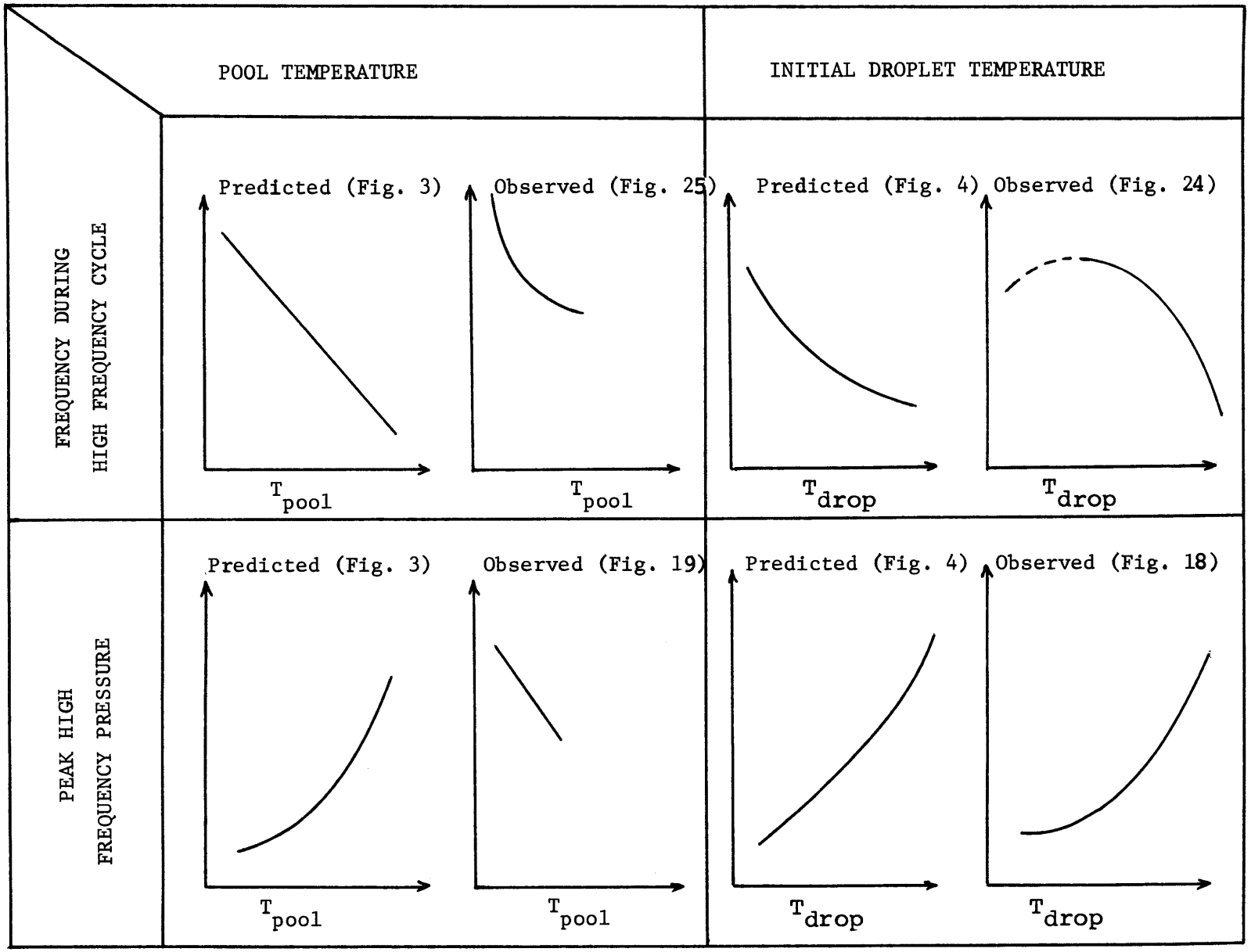

FIGURE 26

COMPARISON OF PREDICTIONS WITH EXPERIMENTAL RESULTS

37 psi (see Table 1), while the experiment gives a value of about 2 psi for the same initial conditions. This quantitative difference can be due to the actual initial film thickness being greater than the thickness of 10^{-5} cm that was assumed in the calculations. Using a thicker initial film has the effect of decreasing the magnitude of the predicted peak pressure, without significantly altering the general qualitative behavior.

A decrease in the film frequency is calculated to result from increasing the initial droplet temperature (see Figure 4). The observed effect, shown in Figure 24 and redrawn in the upper right hand quadrant of Figure 26, is of a decreasing frequency for most of the temperature range, but shows an observed increase in frequency over the temperature range 300°C to 400°C. No satisfactory explanation can be given at present for the disagreement observed at these lower temperatures.

Increasing the droplet temperature is observed to have the effect of increasing the peak high frequency pressure, as is clearly shown by Figure 26. This is in excellent agreement with the calculated trend of increasing peak film pressure with increasing droplet temperature as given by Figure 4. As noted earlier, the calculated peak pressure is roughly an order of magnitude greater than the observed pressure. The same film thickness argument used earlier may be applied here to explain this quantitative difference.

CHAPTER IV

CONCLUSIONS

In this section, the ramifications of the observed pressure behavior are discussed in the context of the acoustic cavitation theory of fragmentation. The observed pressure behavior is then briefly considered in its relation to other proposed theories.

A. Acoustic Cavitation Theory of Fragmentation

It was seen in the previous section that several of the assumptions upon which the film pressure calculations were based deviate significantly from what was observed. In order for the model to accurately reflect the observed initial conditions, the assumption of spherical symmetry of both the droplet and the film must be changed to reflect the irregular geometry of the submerged droplets. Vapor was observed in some of the high speed movies to detach from the trailing edge of the film, and in most cases appeared to be thicker at the trailing edge than at the leading surface. Therefore the assumptions of symmetric film and no vapor escaping from the film are inadequate. In addition, the high observed fall velocity of the droplets through the coolant makes the assumption that the droplet is stationary relative to the coolant over the entire

interaction period a poor one. And finally, the assumption of instantaneous entry was seen to be considerably different from what was observed. Calculations indicate an approximate time of 6 msec for the droplet to completely submerge after a free fall of two inches. Since the peak film pressure is calculated to occur on the first cycle, this last assumption results in a considerable overprediction of the pressure magnitude.

The predicted pressure behavior in the droplet interior was seen to depend strongly on the calculated film pressure behavior. More specifically, the response of the pressure at the droplet center to the film pressure behavior appears to be very strongly dependent on the time and magnitude of the first calculated film pressure peak. It is thought that when the initial film pressure behavior actually observed (less violent than calculated) is used as the surface driving function, significantly less severe pressure excursions will result in the interior of the droplet. Further, doing away with the assumption of spherical symmetry will decrease the observed pressures in the droplet interior because less pressure focusing will occur. It seems clear that the net effect of non-spherical geometry and the less violent film pressure behavior will be much less severe pressure excursions inside the droplet. This would appear to significantly lower the probability that acoustic cavita-

tion will actually occur in the droplet, and would consequently diminish the significance of the role of acoustic cavitation as a mechanism of free contact fragmentation, if not eliminate it completely. More realistic calculations are required to verify this assertion.

B. Jet Penetration Theory

The apparent regular pattern of the pressure records obtained strongly suggests that a single phenomenon is acting. For a fixed coolant temperature there appears to be an initial tin temperature below which the dwell time is relatively constant. This regime is characterized by a short lived (about 1.5 msec) pre-bang high frequency cycle, which is immediately followed by the Big Bang, i.e. the low frequency pressure wave characteristic of the fragmentation event. Above an initial tin temperature of 400°C (for a pool temperature of 21°C) the dwell time increases in an approximately exponential fashion as a function of the initial droplet temperature (see Figure 16). The dwell time period is consistently characterized by a high frequency oscillation that first grows, and then decreases in magnitude. Following the decrease, an abrupt initiation of a new high frequency oscillation is observed to occur. This pre-bang high frequency cycle immediately precedes initiation of the Big Bang.

This regular pattern is strongly suggestive of a phenomenon coupled to the dynamics of an oscillating film. The dwell time might then be a measure of the time required for the droplet to cool to the film collapse temperature. However, this interpretation poses a problem since calculations indicate that no appreciable cooling of the droplet occurs during the period defined by the dwell time (see Appendix B).

Buchanan and Dullforce (8) have considered the dwell time in this context, and have shown that under the assumption of a heat flux from the droplet being proportional to some power of the temperature, the qualitative behavior of the dwell time can be predicted over the range of temperatures investigated (initial tin temperatures to 900°C). Further investigation of the higher temperature regime was recommended to check the applicability of this interpretation.

Further comparison of the results to those of Buchanan and Dullforce leads to an insight to the possible role of the droplet radius in the interactions.

The radius of the droplets was held fixed at 0.3 cm in the present experiments where the fragmentation event was seen to be characterized by a single Big Bang. The experiments of Buchanan and Dullforce (8) involved a larger droplet radius of approximately 0.8 cm, however, and pro-

duced what appeared to be repeated Big Bangs, each separated from the preceding one by a distinct time interval, and with each succeeding Big Bang having a peak pressure greater than that of the preceding one. If it is indeed the larger droplet radius that is responsible for the multiple Big Bang, then the conclusion to be drawn seems clear. For a single droplet of molten tin dropped into water, there must be a limit to the amount of material that can fragment in any single event. Moreover, the effect of increasing the droplet radius is to increase the number of fragmentation events (Big Bangs) that must occur before the tin and water reach thermal equilibrium. More data for varying droplet radii are necessary to elucidate this area, and are scheduled to be obtained this summer.

C. Spontaneous Nucleation of the Coolant

A further point of interest stems from the fact that the nature of the pressure wave accompanying the fragmentation process does not appear to change as the temperature of the droplet is increased from a temperature corresponding to an interface temperature that is below the homogeneous nucleation temperature of the coolant (314°C for H_2O) to a temperature that gives an interface temperature above the homogeneous nucleation temperature. In addition, for a tin temperature of 500°C the interface temperature is approximately 425°C in water at 20°C, and is approximately

420°C in water at 40°C. At both coolant temperatures the interface temperature is well above the homogeneous nucleation temperature of water, and yet extensive fragmentation occurred at 20°C while it did not occur at 40°C. This strongly suggests that spontaneous nucleation of the coolant is not the mechanism of fragmentation of molten tin in water under these conditions.

D. Recommendations for the Future

Further experimental and theoretical work are clearly warranted on the basis of the results obtained in the present work.

In order to accurately relate the pressure records to events observed in the high speed movies, data should be obtained where time reference marks are recorded on both the films and pressure records. Since it appears that the droplet radius may influence the course of the interactions, pressure histories should be obtained for tin and water where the droplet radius is varied. In order to investigate the validity of the interpretation made by Buchanan and Dullforce of the significance of the dwell time, data should be obtained for higher tin temperatures. The last significant experimental task indicated by the present work is the investigation of the effect of using materials other than tin and water on the frequency and magnitude of the pressure waves accompanying the interactions.

The future theoretical work should include an investigation of the magnitude of the heat transfer from the molten droplets to the coolant, particularly in light of the fact that reasonable estimates of the heat transfer rates (see Appendix B) indicate that the droplets do not cool appreciably prior to fragmenting, while on the other hand the assumption made by Buchanan and Dullforce (8) that the droplets do cool significantly prior to fragmenting apparently leads to a qualitatively consistent theory over the range of variables investigated. Further theoretical work should also include a calculation of the pressures in the droplet interiors, using the film pressures obtained experimentally and the model developed by Watson for spherical geometry. Doing so will provide an upper bound on the magnitude of the negative pressures expected in the interior of the droplets, and will provide a more substantive basis for assessing the applicability of the acoustic cavitation theory of fragmentation.

Additional equipment will be required to obtain the required information:

1. A higher temperature furnace;
2. Equipment to provide an inert heating atmosphere;
3. A tape recording device with the capability for recording for longer periods than the maximum of 20 msec allowed by the present unit

(Either modifying the present Ballantine recorder or buying a high fidelity recorder might accomplish this);

4. An analog sampling device to act as an interface between the signal recorder and an XY plotter (to produce accurate pressure traces on paper);
5. A master control panel to allow a single experimenter to control from one location the triggering of all necessary electronics and photographic gear.

APPENDIX A

NOMENCLATURE

α = thermal diffusivity (ft^2/hr)

ε = convergence parameter

ω = angular frequency (sec^{-1})

δ = thickness of vapor film

ε' = emissivity

a = molten sphere radius (cm)

c = velocity of sound (cm/sec)

cs = camera separation (in)

DH = drop height (in)

h = total heat transfer coefficient (Btu/hr ft^2°F)

h_c = convective heat transfer coefficient (Btu/hr ft^2°F)

h_r = radiative heat transfer coefficient (Btu/hr ft^2°F)

k = thermal conductivity (Btu/hr ft °F)

k' = wave number, $k' = w/c - i\,\varepsilon$ (cm^{-1})

OTH = optical trigger height (in)

p(a) = measured pressure at droplet surface relative to p_∞ as calculated using equation (9) (psi)

p(a,t) = absolute calculated film pressure (psia)

p(r) = pressure measured by transducer at distance r relative to p_∞ (psi)

p(r,t) = calculated droplet interior pressure, r<a (psi)

p_∞ = ambient pressure, 14.7 (psia)

$p_\omega(a)$ = Fourier Transform of p(a,t)

$$p(a,t) = \int_{-\infty}^{\infty} p_\omega(a) e^{-i\omega t}\, d\omega$$

r = radius variable (cm)

t = time (sec)

TD = transducer depth (in)

Δt_d = dwell time (msec)

$\bar{v}$ = average fall velocity of molten tin through the water pool (inches/second)

WD = water depth (in)

APPENDIX B

CALCULATION OF DROPLET COOLING DURING THE DWELL TIME

First, a brief calculation was made to investigate the assumption of a uniform droplet temperature. Using h=50 for a 700°C tin droplet in water at 20°C gives a value of the Biot Modulus (18) of

$$Bi = \frac{hR}{k} = 0.026 \ . \qquad \text{(B-1)}$$

This value can be applied to the method presented by Arpaci (18) to show that no significant thermal gradients will exist in the tin droplets, thus justifying the assumption of uniform droplet temperatures in the following droplet temperature calculations.

Under the assumption that constant boundary temperature film boiling is occurring around the spherical droplets, dQ, the heat given up by the tin in time dt can be written as

$$dQ = Ah(T_f - T)dt = mc_p \, dT \quad , \qquad \text{(B-2)}$$

where A is the droplet surface area, T_f is the water temperature, T is the time varying droplet temperature,

m is the droplet mass, and c_p is the specific heat of tin.

Rearranging and integrating equation (B-2) gives

$$\int_{o}^{\Delta t_d} dt = \frac{mc_p}{Ah} \int_{T_o}^{T_{\Delta t_d}} \frac{dT}{(T_f - T)} \quad , \tag{B-3}$$

which can be evaluated and solved for $T_{\Delta t_d}$, the temperature of the droplet after the dwell time (Δt_d) has elapsed:

$$T_{\Delta t_d} = T_f - (T_f - T_o)e^{-\frac{Ah}{mc_p} \Delta t_d} \quad . \tag{B-4}$$

The value of the heat transfer coefficient, h, is calculated using

$$h = h_c + .75h_R \quad , \tag{B-5}$$

where h_c is the convective heat transfer coefficient calculated using the Bromley film boiling correlation, and h_R is the radiative heat transfer coefficient

$$h_R = \sigma\varepsilon' \frac{T^4 - T_f^4}{T - T_f} \quad , \tag{B-6}$$

where σ is the Stefan-Boltzman constant and ε' is the emissivity of molten tin.

Two cases were examined using the above equations to determine the cooling occurring during the observed dwell times. It can be seen from the following table that no appreciable cooling is calculated to occur during the dwell time under the assumed conditions:

Initial Droplet Temp. T_o (°C)	Water Temp. T_f (°C)	Dwell Time Δt_d (msec)	Total Heat Transfer Coeff. h (Btu/ft^2 hr°F)	$T_{\Delta t_d}$ (°C)
500	20	8	37.8	499.3
700	20	52	52.2	693.7

REFERENCES

1. L.C. Witte, et al., "The Vapor Explosion", Journal of Metals 39-44, February 1970.
2. T. Enger and D. Hartman, "Rapid Phase Transformation During LNG Spillage on Water", presented at 3rd International Conference and Exhibition on LNG, Washington, D.C., September 24-28, 1972.
3. L.C. White, et al., "Heat Transfer and Fragmentation During Molten-Metal/Water Interactions", Journal of Heat Transfer, 521-527, November 1973.
4. K. Flory, et al., "Molten Metal-Water Explosions", Chem. Eng. Progress 65, 50-54, December 1969.
5. M.S. Kazimi, "Theoretical Studies on Some Aspects of the Molten Fuel-Coolant Thermal Interaction", MITNE-155, May 1974.
6. H.K. Fauske, "Some Aspects of Liquid-Liquid Heat Transfer and Explosive Boiling", presented at Fast Reactor Safety Conference, Beverly Hills, April 2-4, 1974.
7. D.R. Armstrong, F.J. Testa, D. Raridon, Jr., "Interaction of Sodium with Molten UO_2 and Stainless Steel Using a Dropping Mode of Contact", ANL-7890, Argonne National Laboratory, December 1971.

8. D.J. Buchanan and T.A. Dullforce, "Fuel Coolant Interaction - Small Scale Experiments and Theory", presented at Second Specialist Meeting on Sodium Fuel Interaction in Fast Reactors, Ispra, Nov. 21-23, 1973 (UKAEA Research Group, Culham Lab., Abingdon, Berkshire, UK).

9. S.J. Board, C.L. Farmer and D.H. Poole, "Fragmentation in Thermal Explosions", International Journal of Heat Transfer, Vol. 17, pp. 331-339.

10. M.S. Plesset and R.B. Chapman, "Collapse of an Initially Spherical Vapor Cavity in the Neighborhood of a Solid Boundary", Journal of Fluid Mechanics, 47 (2), 283-290, 1971.

11. C.E. Watson, "Heat Transfer Induced Pressure Fluctuations in the Fuel Coolant Interaction", MITNE-156, Mass. Institute of Technology, August, 1973.

12. L. Bernath, "Theory of Bubble Formation in Liquids", Ind. Eng. Chem. 44, 1310-1313, 1952.

13. A.T.J. Hayward, "Negative Pressures in Liquids: Can it be Harnessed to Serve Man?", American Scientist, 59 (4), 434-443, July-August, 1971.

14. C.E. Watson, private communication.

15. P.M. Morse and K. Uno Ingard, Theoretical Acoustics, 240, McGraw-Hill, New York, 1968.

16. G.M. McCracken, "Investigation of Explosions Produced by Dropping Liquid Metals into Aqeous Solutions", Sect. 3.4 of UKAEA Safety Research Bulletin, Issue 11, Spring 1973.

17. R.N. Lyon, "Liquid Metals Handbook", NAVEXOS, 733, Government Printing Office, Washington, D.C., June 1972.

18. V.S. Arpaci, Conduction Heat Transfer, 298 ff, Addison-Wesley, Reading, 1966.

19. Cho, D., W. Gunther and D. Armstrong, "Fragmentation of Molten Materials Dropped into Water", ANL/RAS 73-8, April 1973 (Limited Distribution Report).

20. S.J. Board et al., "Fragmentation in Thermal Explosions", Central Electricity Generating Board Report RD/B/N2423, Oct. 1972.

21. D. Cho, private communications, January 1972.